Available online at www.sciencedirect.com
ScienceDirect
Procedia Computer Science 00 (2012) 1–32
Procedia Computer Science

Dynamic Power Distribution and Energy Management in a Reconfigurable Multi-Robotic Organism

Humza Qadir Raja[1a], Oliver Scholz[b]

[a]dSPACE GmbH, 33102 Paderborn, Germany
[b]Department of Measurement Technology, University of Applied Sciences (HTW), 66117, Saarbruecken, Germany

Abstract

Several design parameters in collective robotic systems have been investigated and developed in order to explore the cooperation among the autonomous robotic individuals in a variety of robotic swarms in the presence of different internal and external system constraints. In particular, the dynamic power management and distribution in a multi-robotic *organism* is of very high importance that depends not only on the electronic design but also on the mechanical structure of the robots. It further defines the true nature of the collaboration among the modules of a self-reconfigurable multi-robotic organism. This article describes the essential features and design of a dynamic power distribution and management system for a dynamically reconfigurable multi-robotic system. It further presents the empirical results of the proposed dynamic power management system collected with the real robotic platform. In the later half of the article, it presents a simulation framework that was especially developed to explore the collective system behavior and complexities involved in the operations of a multi-robotic organism. At the end, summary and conclusion follows the detailed discussion on the obtained simulation results.

Keywords: Reconfigurable robotic systems, dynamic power management, energy sharing, energy autonomy, self-sufficiency

1. Introduction

The concept of reconfigurability has been explored in several research areas such as, reconfigurable computing [1, 2], control reconfiguration [3], reconfigurable robotic systems [4], etc. Reconfigurable robotic systems that has been in research focus especially in past couple of decades, at one end show great deal of advantages over traditional robotic systems while on the other end involves several degrees of complexity. One of the main challenge that is still in research focus in different reconfigurable robotic systems employed for different applications deals with the longevity of autonomous reconfigurable robotic systems.

Energy autonomy or *self-sufficiency* is the ability of a mobile robotic system to autonomously regain its replenished energy from the environment to prolong its operations for a longer period of time [5]. According to Ngo [6], the first norm of "autonomy" affirms that self-sufficient robots must have some degree of freedom in order to maintain their energetic status in equilibrium along with their essential assigned tasks in the environment. The second norm allegedly asserted that the external factors that are beyond the control of an autonomous robot in fact limit its self-sufficiency.

[1]was formally with Biomedical Micro-systems Department, Fraunhofer Institute for Biomedical Engineering (IBMT), 66386 St. Ingbert, Germany, rajahamza@gmail.com

The factors that play a critical role in maintaining the energy autonomy of an artificial autonomous robotic system can then be classified into two categories: internal – system dependent, and external – environment dependent.

Later, Yuta and Hada proposed a bench-mark to achieve long term autonomy in autonomous robotic systems [7]. They considered the autonomy of a robot on both layers: hardware and software. The hardware or physical autonomy is linked with an individual's abilities to perform multiple task e.g., mobility with a self-contained body, self-healing or self-renovation, without any external intervention. Whereas, the autonomy of a robotic system at software layer is defined as its adaptive ability in decision making, learning and behavior acquisition in an unstructured dynamically changing environment.

The autonomy at higher layers in a reconfigurable multi-robotic system cannot be realized without gaining or having the autonomy at lower or physical layer. For similar reasons, the energy autonomy of an individual robotic module in swarm and organism mode, requires dedicated dynamic power management features embedded in the system design. The physical layer power management functions then empower the application layer software to control and coordinate a robot's behavior with other robotic entities and its surrounding environment.

The internal factors that are critical in gaining the energetic autonomy to an autonomous individual solely depends on its mechanical and electronic architecture. It includes, firstly, the control over its movement, i.e., how much power actuators require to cover a certain distance. Since the rest of a module's functionalities/abilities are directly or indirectly dependent on its movement in the arena. In literature, several approaches have been reported on efficient motion planning that try to reduce the overall power consumption. Barili et. al. tried to control the robot velocity with respect to the path planning for optimizing energy consumption [8]. Silva and Machado characterized the motion of the system in terms of a set of locomotion variables, namely: step length, hip height, hip ripple, hip offset, foot clearance and link lengths, to minimize energy consumption of mobile robots [9]. A similar control algorithm was presented by Yamasaki et. al. in [10] that reduces the power consumption of a humanoid robot. Duleba and Sasiadek presented a modification of the Newton algorithm applied to nonholonomic motion planning with energy optimization [11] . Mei et. al. used models of motor friction and events of robot turning and stopping for energy efficient motion planning for mobile robots [12]. They also proposed in [13], an algorithm that uses orientation-based target selection to reduce the repeated coverage to save significant portions of energy. Second critical factor in gaining the energetic autonomy includes the module's sensing ability, that is very much dependent on different sensing tools it own, e.g., microphone, vision system, laser, etc. The sensing tools help an autonomous robot to cost effectively search, detect and locate power sources by avoiding unwanted obstacles in the arena. Thirdly, an individual's ability to self-regulate or adapt it's behavior/operations with the available on-board energy reserve. For instance, if the movement in the arena for a robotic module is getting expensive from power consumption perspective then it may limit or fully stop it's further movement in the arena for the purpose of energy conservation and wait for other modules to help it. And last but not least, the ability of a system to withstand abrupt system failures – fault tolerance. For instance, an instant short circuit may ruin the whole electronics. With having innate fault tolerance – embedded at the physical layer, a module may save itself from unpredictable break downs/system failures and may not affect other robotic modules when physically docked to them.

In swarm robotics, the external factors that are important for an autonomous individual in maintaining its energy autonomy mainly depend on the energy availability in the environment. The availability of energy in the environment further involve different parameters that may include number of power stations (energy sources) in the arena, number of competitors that are varying with time in case of a swarm [14], and the obstacles that an autonomous individual may encounter in reaching a power station.

This work is organized as follows: Section 2 briefly describes the state of the art reconfigurable robotic platforms from energy sharing perspective. Section 3 presents the deficiencies found in the existing state of the art multi-robotic systems again from power management and energy sharing perspective. Section 4 discusses the system/platform dependent parameters in the design of a dynamic power management and energy sharing system. Section 5 presents the state of the art REPLICATOR robot's electronic architecture. Section 6 then presents the hardware design of a dynamic power management and energy sharing system designed for REPLICATOR robotic modules. Section 7 presents the experiments performed with real REPLICATOR robotic platform. Section 8 presents the simulation framework designed to explore the collective system behavior in different scenarios and discuses the simulation results. And finally, Section 9 concludes the work with summary and conclusion.

2. Related Work

This section briefly reviews the design of state of the art reconfigurable robotic systems that allow power management and energy sharing. In this regard, we have chosen two state of the art reconfigurable multi-robotic systems: SuperBot and ATRON. These two robotic systems are selected as examples for our research work because with these a basic concept of power management and energy sharing has already been demonstrated to the reconfigurable robotics research community.

2.1. SuperBot

The SuperBot is a multi-functional, autonomous, reconfigurable, homogeneous modular robot designed and developed by the University of Southern California (USC) [15]. The form factor of SuperBot module is a bit similar to the M-TRAN modules [16]. The salient features of a SuperBot robotic platform include, three degrees of freedom (DOF) – yaw, pitch, and roll, high-speed infra-red LEDs, power sharing, re-configurability and flexible design that enables the dynamic configuration of modules to perform efficient locomotion and task manipulation. The mechanical design of a SuperBot robotic module comprises on two halves. One half of the module contains a battery pack, a motor drive, control mechanism for three docking sides i.e., M1, M2, and M3, and a central controller called the "master controller". The master controller is connected to the controller of the second half, called the "slave controller". The

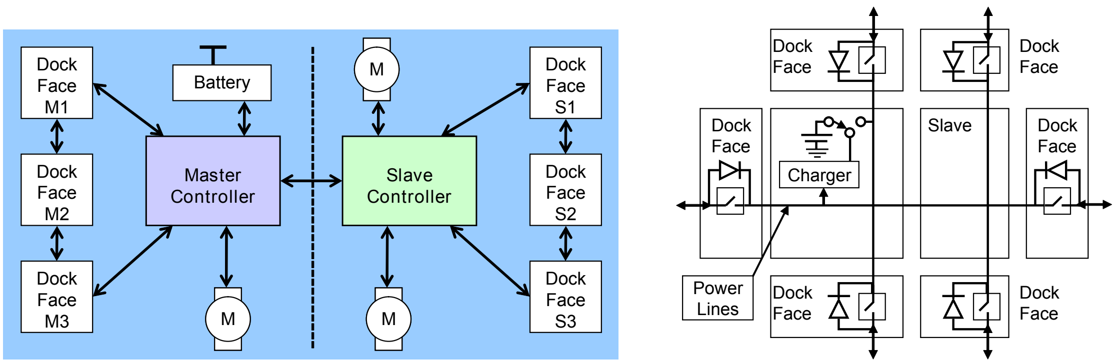

(a) (b)

Figure 1: SuperBot platform [15]: (a) Block diagram of the hardware control architecture, (b) SuperBot power sharing schematic

two controllers in each half are therefore responsible for managing the operations of actuators, communication links, sensors, power flow and the docking interfaces on each respective side. Fig. 1a shows the block diagram of hardware control architecture of a SuperBot module. Each module has 6 docking connectors (sides) to allow the physical docking to other robotic modules in different configurations.

From power management perspective, each module is powered by two serially connected lithium polymer cells (2s1p) that provide a nominal voltage of 7.4 volts with a charge capacity of 1600 mAh, [15]. Fig. 1b shows the SuperBot power sharing schematic. It includes 6 docking interfaces (3 on each half), and a recharge mechanism. At each docking interface, a diode allows a uni-directional – inward, current flow into the system. Whereas the outward current flow was actively controlled by the controller on each lateral side using a switch present on each docking interface. Further, the local power bus interconnects the 6 docking interfaces thus allowing a omni-directional power flow in the system.

In the default system state the charging switch i.e., the switch that connects the battery with the charging module, remains closed while the rest of the switches – on each docking interface, remain open. Upon the application of an external power source on any one of the docking interface in the default configuration of power bus switches, allows the power to flow into the system's recharging module thus allowing the on-board battery to recharge, instantly. This configuration of power bus switches in a multi-robotic organism thus allows the turn-by-turn recharging of several modules in an organism (in case, all the modules are dead) when any one of them is connected with an external power

source. The power bus in a SuperBot multi-robotic organism not only allows the recharging of robotic individuals through the external power source but also allows them to share their energy with each other.

2.2. ATRON

The ATRON is a self-reconfigurable modular robot originally developed by the Adaptronics group at the University of Southern Denmark (USD) [17]. An ATRON robotic module consists of two hemispheres, joint together by a rotating mechanism, which provides one DOF (degree of freedom) to the mechanical design. Each hemisphere has two passive female connectors and two active male connectors which enable a module to hook/dock to the complementary female connectors of the docking module [18]. This design of the center allows a module an infinite number

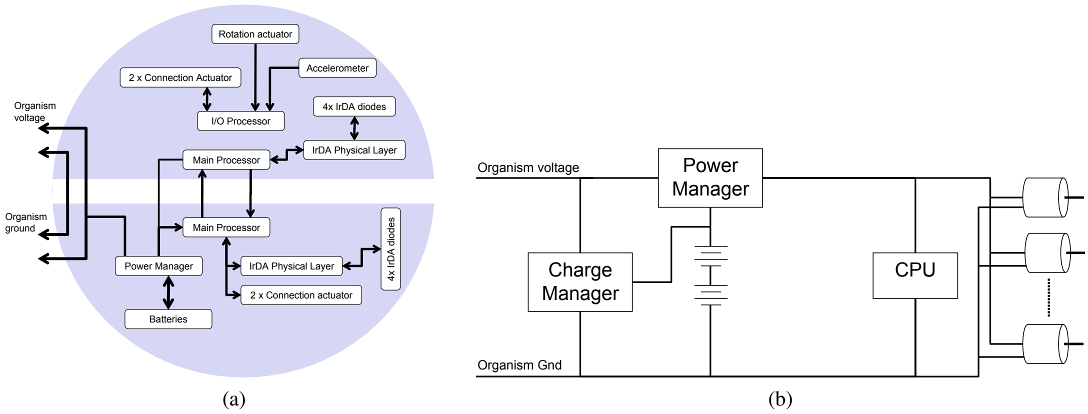

Figure 2: Homogeneous ATRON robotic system [19]: (a) Block diagram of the electronics in an ATRON module. The northern hemisphere contains an accelerometer, a rotation actuator, four IrDA diodes, an I/O processor, and a main processor. The southern hemisphere contains a main processor, a power manager, a battery pack, actuators, and 4xIrDA diodes. (b) ATRON module's power management system

of revolutions around the equator while still transferring power and data between the two hemispheres. Not only that, the two four-sided pyramids with craving allow the free rotation of modules with an ATRON organism.

From the system electronic design perspective, each hemisphere of the ATRON module has one 8-bit 16MHz ATmega128 micro-controller. Fig. 2a shows the block diagram of electronics in an ATRON module. The northern hemisphere contains a main processor, an I/O processor, two docking connectors, a rotation actuator, an accelerometer, and four IrDA diodes. The southern hemisphere in addition to the main processor includes, a power manager, a battery pack, four IrDA communication diodes, and two active male connectors. The controller in the southern hemisphere is responsible for inter-organism power sharing, recharging of on-board battery pack, communication through four IrDA channels and controlling two active male connectors. Further, each module is energized by two serially connected lithium-polymer cells (2S1P) that provide the nominal voltage of 7.4 V with a max. charge capacity of 980 mAh [19].

To maintain consistent power supply to all of the robotic modules in an organism the ATRON module's electrical skeleton enables the multiple modules to share / transfer their power among each another. This also allows the modules to recharge the neighboring module's battery pack. For this purpose, the entire supporting metal structure forming the skeleton of an ATRON module is electrically grounded. For transferring positive voltage, one of the docking hook has an electrically insulated piece of flexible printed circuit board glued on top of it, that allows the module to form power bus when are physically connected [19].

Fig. 2b shows the power management system of an ATRON module. It includes a power manager, a charge manager, battery cells, and a CPU. As described in [19], the *power manager* in the system is mainly responsible for monitoring the on-board battery pack supply voltage and the voltage across the organism's power bus to select the best suited power source to power up its on-board electronics. The power / energy sharing in a module is triggered if the organism's voltage (voltage across the power bus) is below a certain threshold with respect to the on-board battery pack's voltage. For collective recharging, i.e., parallel recharging of multiple modules in an organism, because of the common power bus it is sufficient to connect a single module to an external power source. When docked to

an external power source – recharge station, the modules then by election decide who gets to re-charge its battery pack first. A critical parameter that determines the maximum number of recharging modules in an organism is the maximum amount of instantaneous current that can flow through the organism's power bus. The ATRON module's system design allows a maximum of 7 A of current to flow through the docking contacts. Therefore, 500 mA of recharge current allows a maximum of 14 ATRON modules to recharge themselves simultaneously in an organism.

3. Deficiencies in the Existing State of the Art Multi-Robotic Systems

This section point out some of the essential system features concerning power management and energy sharing required for the dynamic collaboration of robotic modules in an organism. After having a detailed analysis of the state of the art reconfigurable multi-robotic systems, the following features may be found to be missing in existing systems. They are not able to:

1. determine/measure the current flowing through the on-board battery pack to system peripherals and to each docking interface – to the docked modules in the organism,
2. withstand abrupt system failures, such as, a short circuit,
3. actively control the recharging of on-board battery pack in organism mode especially in case of a faulty battery pack,
4. dynamically control the current flow through the organism's power bus – among the modules of an organism.

Measuring the current flow: The current flow measurements / readings at the critical system segments play an important role in controlling the dynamic operations of any battery operated autonomous mobile robotic system. These measurements allow a system to predict system malfunctions/failures even before they occur. The current flow measurements also help the robotic modules to efficiently utilize the available energy distributed in the organism.

Abrupt System Failure: An important ingredient in the electro-mechanical design of any autonomous system is its ability to withstand abrupt system failures. From dynamic power sharing perspective, the system design must have an innate fault tolerance, e.g., current limiters, fuses, switches, etc., to withstand abrupt short circuiting during the normal operational mode of a robotic module.

Control over the current flow through the organism's power bus: The control over the current flow path in a multi-robotic organism, where at one end provides adaptive fault tolerance ability to individual and collective systems, on the other hand, allows the modules to efficiently utilize the available battery power in the organism, i.e., by forming sub-power buses.

4. System Dependent Parameters

The above section briefly highlights some of the essential features of a dynamic power distribution and energy management system required for the dynamic collaboration of multiple modules in an organism. Keeping in view such desired system features this section point out the decisive system dependent, i.e., on the electro-mechanical design of a robotic module, parameters that are involved in the hardware design of an individual's power management system.

In the electronic design of a mobile autonomous system, the critical system components that are effected by a robot's mechanical architecture include, firstly, the on-board space available for the battery pack. And secondly, the mechanical connectors responsible for establishing power bus at the docking interfaces of two physically docked robots. The on-board space available for a battery is critical, since in case of a rechargeable Lithium-Ion battery pack it directly determines its charge capacity typically measured in milli-Ampere hour (mAh) and its terminal voltage. The terminal voltage of a rechargeable lithium-Ion battery pack depends upon the number of serially connected cells and its charge capacity depends on the cell's size. The mechanical connectors are another influential component of the system design since their selection where at one end is highly dependent on the mechanical construction of a robotic platform, on the other end, directly influences the electrical characteristics of the whole system, i.e., the amount of current that can flow between the two docked robotic modules.

Concerning the hardware design of an autonomous robotic system having power sharing ability, the most significant parameter is the system voltage i.e., battery pack voltage. As it's influence appears on several system components, e.g., the components that are available in market operating in the particular voltage range, the current flow through the organism's power bus, i.e., a low system voltage induces high current flow through the organism's power bus, consequently high power losses and vice versa, etc. Other consideration in regards to system voltage includes, how much current

- will be required to flow through the organism's power bus?
- the docking connectors can withstand?
- is safe to flow through the organism's power bus, i.e. the upper limit that ensures the steady state operation of robotic modules within an organism?
- or power can a robot donate/share to other docked robots in the organism?

Theoretically, these parameters can be chosen arbitrarily. But in a real system design they may limit certain essential capabilities of an autonomous system.

5. Replicator Robot Electronic Architecture

The REPLICATOR robots bears heterogeneous platform design that includes backbone, scout, and active wheel robot [20]. Irrespective of the mechanical architecture, each REPLICATOR robotic module carries some homogeneous components, i.e., that are common among the three platforms, with additional heterogeneous components that in fact define its unique abilities.

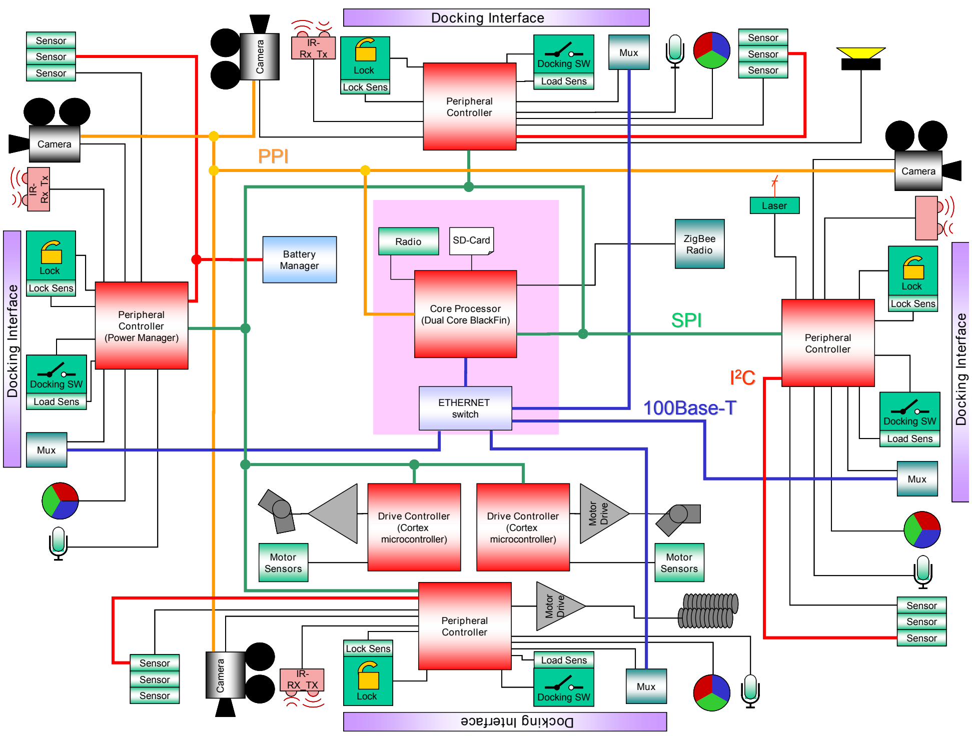

Figure 3: Electronic architecture block diagram that is common on the three REPLICATOR robotic platforms: backbone robot, Scout robot and active wheel [20].

Fig. 3 shows the block diagram of electronic architecture that is common on the three REPLICATOR robotic platforms. To fully and efficiently utilize the system capabilities the electronic architecture of a REPLICATOR module was divided into two control units i.e., the "core" processor and the "shadow" or "peripheral" controllers. The *core processing unit* on each robotic platform is a *CM-BF561* drop-in module from BLUETECHNIX equipped with a dual core *Blackfin BF561* μcontroller from ANALOG DEVICES. Via a Serial Peripheral Interface (SPI), this unit is attached to 4 peripheral μcontrollers (*MSP430F2618* from TEXAS INSTRUMENTS), which are responsible for sensor data acquisition, low level actuator control and processing in order to take off burden from the main processing unit. These peripheral controllers mainly serve as an interface between the application software routines running on the *Blackfin* processor and the system components. All μcontrollers and corresponding peripheral elements are placed on separate PCBs, installed on each side of a robot module. Each of these PCBs have in common certain sensors and actuators (e.g. docking sensors and actuators, microphones, RGB-LEDs, etc.), but may in addition take over specialized tasks (e.g. 2D or 3D locomotion, ZigBee radio interface, etc.). For 3D actuation, up to two additional *LM3S8962 Cortex* μcontrollers (LUMINARY MICRO) are integrated to permit high-performance brushless DC-motor control. On each of the PCBs, a local I^2C bus is implemented for interfacing the local controller with the respective sensors. In addition, a global I^2C bus has been implemented to facilitate multi-master communications between the peripheral controllers.

5.1. Choice of Source Voltage

The *system voltage* is the battery pack voltage that becomes the source voltage to all of the system components. A direct impact of the system voltage on the overall system energetic efficiency can be seen at step up/down voltage regulators. A step up voltage regulator or boost converter is required in case the source voltage is below the nominal voltage required to drive a component. Similarly, on the other side, if the source voltage is too high then the step down voltage regulator or buck converter brings down the system voltage to the nominal voltage required. Another impact of a low system voltage appears in the form of high current flow through organism's power bus during energy sharing.

Table 1: Transformed current consumption of individual components with three different on-board power sources, i.e., 7.4 V, 11.1 V, and 22.2 V.

Components	Curr. transf. w/t 7.4 V		Curr. transf. w/t 11.1 V		Curr. transf. w/t 22.2 V	
	nomical	Peak	nominal	Peak	nominal	Peak
2-D locomotion drive	389.19	1212.97	259.46	808.65	129.73	404.32
2-D drive controller	29.43	49.05	19.62	32.70	9.81	16.35
3-D hinge drive	2378.38	5945.95	1585.59	3963.96	792.79	1981.98
3-D drive controller	29.43	49.05	19.62	32.70	9.81	16.35
Drive retraction	316.22	1277.84	210.81	851.89	105.41	425.95
4x docking drives	316.22	1277.84	210.81	851.89	105.41	425.95
Laser scanner	17.84	22.30	11.89	14.86	5.95	7.43
ZigBee module	7.14	17.84	4.76	11.89	2.38	5.95
4x docking sensors	17.84	89.19	11.89	59.46	5.95	29.73
4x RGB status LEDs	53.51	142.70	35.68	95.14	17.84	47.57
Localization unit	0.90	67.57	0.60	45.05	0.30	22.52
Core processor	45.93	211.82	30.62	141.22	15.31	70.61
4x μ controllers	10.79	11.15	7.19	7.43	3.60	3.72
Ethernet module	337.58	434.80	225.05	289.86	112.53	144.93
4x Vision sensors	8.03	8.92	5.35	5.95	2.68	2.97
Power Mngt. module	15.0	20.0	15.0	20.0	15.0	20.0
Batt. Mngt. module	1.0	1.0	1.0	1.0	1.0	1.0
Total curr. consumption	3974.2	10838.74	2654.8	7232.50	1335.4	3626.25

To calculate the impact of system voltage on the overall system instantaneous current consumption we have transformed the individual current consumption of the components with different source voltages. Table 1 shows the current consumption of individual components that was transformed to three different voltage levels. The chosen

power sources are the different combination of serially connected LiPo cells, e.g., a 2S1P configuration denotes a combination of 2 serially connected cells that provide a nominal voltage of 7.4 V. The first two columns, i.e., two and three, in table 1 show the transformed current consumption of the individual components with a voltage source of 7.4 V. With a 7.4 V source voltage the typical current consumption of the system components when all them were in active state summed up roughly between 4 Amps to 11 Amps, at most. The next two columns, i.e., fourth and fifth, in table 1 show the measurements made with a voltage source of 11.1 V. With a 11.1 V voltage source the instantaneous system current consumption varies between 2.6 Amps to 7.2 Amps. Finally, the last two columns in table 1 show the transformed current with a source voltage of 22.2 V. With a 22.2 V voltage source the overall system current consumption varies between 1.3 Amps to 3.6 Amps. Keeping in view, these theoretical measurements do not include any efficiency measure, such as, the efficiency of step-up/boost and step-down/buck voltage regulators, current losses at docking interfaces, etc.

Table 2: Current consumption of a REPLICATOR robotic module operating in swarm and organism mode with three different on-board source voltages

Components	Duty cycle		Op. Curr. at 7.4 V		Op. Curr. at 11.1 V		Op. Curr. at 22.2 V	
	Swarm	Org.	Swarm	Org.	Swarm	Org.	Swarm	Org.
2-D loco. drive	0.9	0.5	350.27	194.59	233.51	129.73	116.76	64.86
2-D drive contr.	0.9	0.0	26.49	0.00	17.66	0.0	8.83	0.0
3-D hinge drive	0.0	0.5	0.0	1189.19	0.0	792.79	0.0	39.40
3-D drive contr.	0.0	0.5	0.0	14.72	0.0	9.81	0.0	4.91
Drive Retraction	0.5	0.5	158.11	158.11	105.41	105.41	52.70	52.70
4x docking drives	0.2	0.2	63.24	63.24	42.16	42.16	21.08	21.08
Laser scanner	0.3	0.3	5.35	5.35	3.57	3.57	1.78	1.78
ZigBee module	0.8	0.5	5.71	3.57	3.81	2.38	1.90	1.19
4x Docking Sensor	1.0	1.0	17.84	17.84	11.89	11.89	5.95	5.95
4x RGB LEDs	0.5	0.5	26.76	26.76	17.84	17.84	8.92	8.92
Localization unit	1.0	1.0	0.90	0.90	0.60	0.60	0.30	0.30
Core processor	1.0	1.0	45.93	45.93	30.62	30.62	15.31	15.31
4x μ controllers	1.0	1.0	10.79	10.79	7.19	7.19	3.6	3.60
Ethernet module	0.0	1.0	0.0	337.58	0.0	225.05	0.0	112.53
4x Vision sensors	0.5	0.5	0.0	0.0	0.0	0.0	0.0	0.0
P. Mngt. module	1.0	1.0	15.00	15.0	15.0	15.0	15.0	15.0
B. Mngt. module	1.0	1.0	1.0	1.0	1.0	1.0	1.0	1.0
Total current (mA)			726.38	2083.57	489.26	1394.04	252.13	704.52

The measurements obtained in table 1 provide a rough estimate of instantaneous current consumption of a robotic module with different on-board voltage sources irrespective of the battery pack charge capacity. To obtain a more precise estimate of a system's instantaneous current consumption in the two operating modes, i.e, swarm and organism mode, an important parameter that is left over in the measurements shown in table 1 is the inclusion of duty cycle i.e., a rough estimate of how long a particular component was required to be in its active or inactive state in relation to the operating mode of a robot.

For this purpose Table 2 provides the measured current consumption of a REPLICATOR robotic module operating in swarm and organism mode again with three different on-board voltage sources. The second column in the table from left shows the duty cycle of individual components that were possibly active in swarm/standalone mode of a robot. The inclusion of duty cycle helps to theoretically estimate the overall system current consumption by assuming the component's active time. For instance, the duty cycle "0" of the 3-D hinge drive shows its permanent inactive state during the swarm mode operations of a robot. In swarm mode with a 7.4 V voltage source the instantaneous system current consumption was $\approx$ 700 mAmps and in organism mode it goes upto 2 Amps. In second case, with a 11.1 V power supply the instantaneous system current consumption reduces to $\approx$ 500 mAmps and in organism mode it again decreases to 1.4 Amps from 2 Amps in comparison with the former case. Finally, with a 22.2 V power supply, the

instantaneous system current consumption further reduces to ≈ 250 mAmps in swarm mode and in organism mode it further reduces to approximately 700 mAmps.

Table 3: Operational time of a REPLICATOR module with three different power sources each having a charge capacity of 1000 mAh and of 75% efficiency

	Oper. Time with 7.4 V		Oper. Time with 11.1 V		Oper. Time with 22.2 V	
Time / Mode	Swarm	Organism	Swarm	Organism	Swarm	Organism
in minutes	61,95	21,59	91,97	32,28	178,48	63,87
in hours	1,03	0,35	1,53	0,53	2,97	1,06

As already stated, a desired element in the design of a battery operated mobile robotic system is its operational time that depends on its instantaneous current consumption, on-board source voltage and the battery pack capacity. Table 3 provides an estimate of operational time of a REPLICATOR robotic module with three different power sources each having a charge capacity of 1000 mAh and of 75% efficiency. From the calculations, a REPLICATOR robotic module with a 2 cells Li-Poly battery pack (2S1P), can operate in swarm mode for about an hour and in an organism mode for ≈ 35 minutes. A REPLICATOR robotic module with 3 cells Li-Poly battery pack (3S1P) can operate in swarm mode for ≈ 92 minutes. and in organism mode for ≈ 32 minutes. Lastly, a module with 6 cells Li-Poly battery pack (6S1P) can achieve a maximum operational time in swarm mode, i.e., ≈ 3 hours, and in organism mode for ≈ 1 hour.

Considering all the calculations made above, i.e., system power budget, choice of the system voltage, system specific constraints, on-board space on the robotic platform available for the battery pack, the estimated operational time and the available battery capacities in market, we have chosen a battery pack of 6 Li-Polymer cells. The chosen battery pack with 6 Li-Poly cells provides the nominal voltage of 22.2 V with a maximum charge capacity of 1050 mAh.

6. REPLICATOR's Power Management System – Hardware Design

After selecting the system voltage, the next step was the design of dynamic power management system with energy sharing ability. The proposed REPLICATOR robot's dynamic power management system design includes all the missing features that are explicitly elaborated in Section 3. The design not only includes the desired features in the hardware design but also provides a higher layer access to application software components to control the dynamic behaviour of an autonomous system. Fig. 4 shows the block diagram of the proposed power management system. It includes a battery management module, a battery re-charging unit, ideal diodes for uni-directional low loss current flow, a system power manager, an energy sharing module, a high power control switch for powering on-board peripherals, and four docking interfaces one on each lateral side of the robot.

6.1. Battery management module:

The battery management module (BMM) consists of two modules, i.e., an analogue front end and a battery controller. The analogue front end (AFE) is a 5–10 series cell Lithium-ion battery pack protector, i.e., *BQ77pl900*, that serves as an AFE in host control mode from Taxes Instrument. It is responsible for managing and controlling the operation of six cells lithium polymer battery pack, for instance charging and discharging, measuring individual cell voltages, cell balancing, over-charge and discharge protection, etc. The battery controller is a 16-bit ultra-low-power μcontroller, i.e., *MSP430F2132*, form Taxes Instrument (TI) for managing the operations of AFE in host control mode. It keeps track of battery pack charge capacity/remaining capacity, the discharging / charging current, individual cell voltages during cell balancing, etc. It also provides an interface to the application layer software components to access and control the operations and capabilities of AFE in a controlled manner.

6.2. Power manager:

The system power manager is a core control module in power management system, that is a 16-bit ultra-low-power *MSP430F2618* μcontroller from TI. It is dedicated to control and monitor the different system functionalities and parameters, respectively, such as, communication with the BMM to extract and control the battery pack parameters,

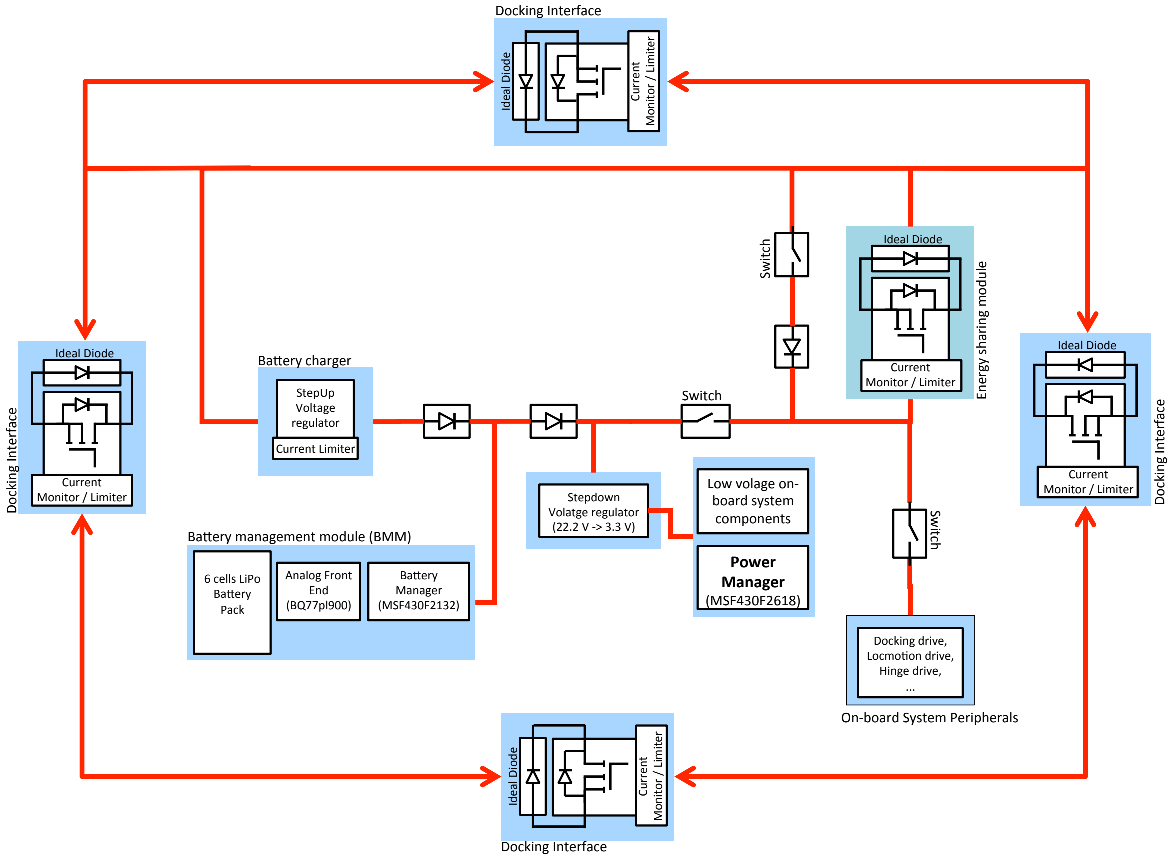

Figure 4: Block diagram of the proposed power management system for a REPLICATOR robotic module

enable or disable power to various on-board system components, e.g. actuators, sensors, docking switches, energy sharing, etc. Not only that, it also measures the current flow through the energy sharing module and the four docking interfaces. These current flow measurements are then transferred to the core processing unit, i.e., *Blackfin* controller, in order to provide an access to the application layer software routines to control the dynamic current flow collectively through the organism's power bus.

6.3. Battery charger

The dedicated battery charger is a DC/DC controller that operates as a constant-current and constant-voltage regulator (LT3756) from Linear Technology. It provides two important features in a single chip, namely, the built in boost converter and the current limiter. The boost converter is required to support the concept of *energy trophallaxis* – recharging an energetically weaker robot by a healthy robot, at hardware layer. And secondly, to protect the battery pack against excess charging current the current limiter is required to limit the charging current during energy trophallaxis.

In the system, when it gets activated by the system power manager, it acts as a constant current, voltage limited source to the battery pack. To reduce the energy losses during energy trophallaxis, in the current configuration, the charge current is limited to 0.5 C flowing into the battery pack. Here, 1C corresponds to maximum charge capacity of the cell, i.e., 1,050 mA.

6.4. Ideal diode

To improve the energetic efficiency of the system, the *ideal diode*, i.e., LTC4358 from Linear technology, reduces the power dissipation by replacing a power Schottky diode with an internal 20mOhm N-channel MOSFET. The device

is mainly used because of its low power consumption, low heat dissipation, high current flow, a small foot print and last but not least, smooth switch over without oscillations.

6.5. Energy sharing module

Energy sharing module in the system allows a module to control the outward current flow, i.e., from the on board battery pack, to other docked modules through the respective docking interface. It is a combination of an ideal diode, a current limiting switch, and a current sensor. The "ideal diode" creates a forward path for the current flowing through the docking interface to the on-board system peripherals. The "current limiter" (CL) not only sets an upper limit on energy sharing but with a MOSFET also acts as switch to control the outward current flow, i.e., from the on-board battery pack to the docking interfaces.

More explicitly, in its *inactive* state, the power bus current may energize the on-board system components if the on-board battery voltage is lower than the voltage across the power bus. While in its *active* state, the CL in the energy sharing module adds an innate fault tolerance ability to the system by limiting the outward current flow to 1.9 Amps.

6.6. Docking interface

The REPLICATOR docking interface is a combination of an ideal diode, a current limiter and a current sensor. On each lateral side of the REPLICATOR robot, the docking interface switch in its default i.e., *inactive*, state provides a uni-directional current flow, i.e., into the system. Whereas, in its *active* state, it provides a bidirectional current flow path through the particular docking interface. At each docking interface, the current sensor MAX9928F, i.e., uni-/bidirectional, high-side, current-sense amplifier by Maxim, allows the system power manager to measure the current flowing through it, and the current limiter TPS2491, i.e., a positive high-voltage, power-limiting hot swap controller by TI, limits the current flow to approx. 8 Amps.

7. Experiments with REPLICATOR Robots

To test the operations of the proposed power management system in a multi-robotic organism at the hardware layer, we had used four prototype version of REPLICATOR Backbone robots. In the experiment setup the robots were physically docked to each other in the form of a chain. Fig. 5 shows the experimental setup in which the Backbone robots were additionally connected with external power supplies that also serve the purpose of electronic load in the system. To read out the current measurements carrying out in the organism, each robot periodically transfers its local system measurements to a PC connected via a UART interface.

The experiment section is divided into two phases: the first phase explains the test scenario and the power sharing measurements captured using REPLICATOR hardware. The second phase introduces a simulation framework especially developed in the light of the experience gained in the first phase to further explore the system capabilities and behavior in different scenarios and configurations.

7.1. Dynamic Power Sharing

For the collective self-sufficiency of autonomous robotic modules in an organism an important design feature embedded in the proposed power management system is its ability to actively monitor and control the power flow in and out of the system, i.e., through energy sharing module and the four docking interfaces.

Fig. 6 shows the block diagram of a power bus established between four REPLICATOR robotic modules that are physically docked to each other, as shown in Fig. 5. At each robotic individual, the system *power manager* measures the inward and outward current flow at the energy sharing module and the four docking interfaces. Consider, I_a, I_b, I_c, and I_d are the variables representing the current flow through the respective docking interface. The variable I_E represents the amount of current that either flows from the battery pack as I_{Batt} to the power bus – energy sharing –, or is consumed by the on-board system components, as I_{sys}, from the power bus.

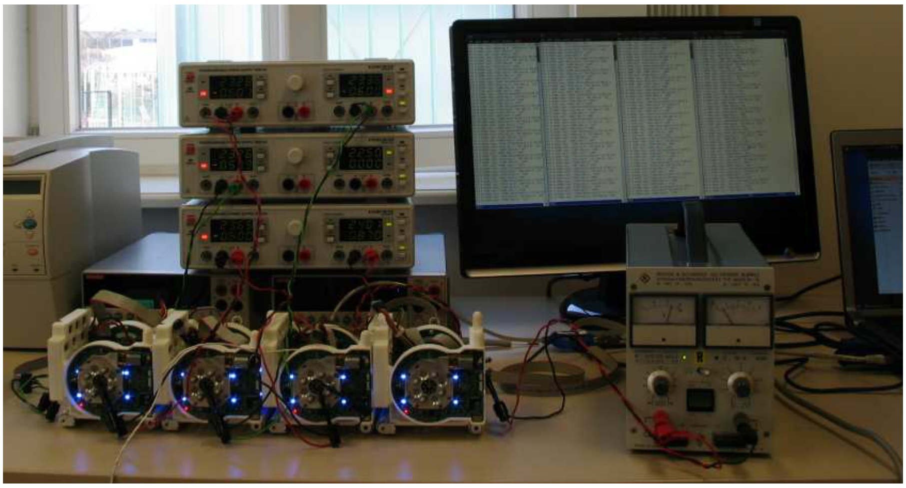

Figure 5: Experimental setup: 4 prototype version of REPLICATOR Backbone robots were docked to each other in the form of a chain. For a controlled power flow through the organism's power bus, the robots were connected with external power supplies that also act as electronic load to the system. The log – current measurements, from each robot were recorded locally and then transferred to a PC connected through a UART interface.

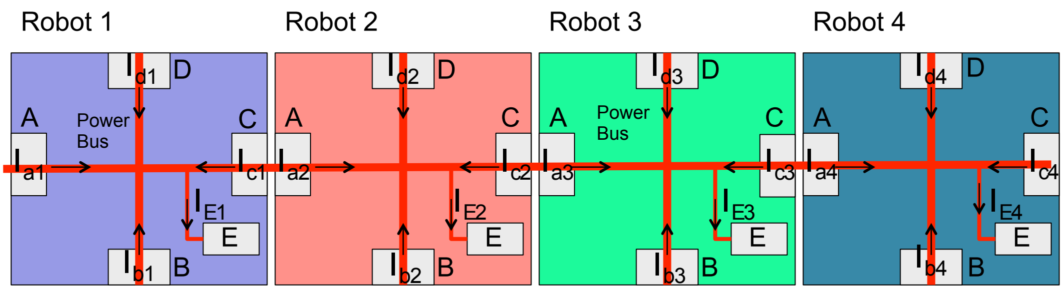

Figure 6: Block diagram of the organism's power bus established between four REPLICATOR robotic modules

To obtain current flow through the organism's power bus, using Kirchhoff's current law, the current flowing through the four sides of robot 1 can be obtained as,

$$I_{a_1} = I_{E_1} - (I_{b_1} + I_{c_1} + I_{d_1}), \quad (1)$$

$$I_{b_1} = I_{E_1} - (I_{a_1} + I_{c_1} + I_{d_1}), \quad (2)$$

$$I_{c_1} = I_{E_1} - (I_{a_1} + I_{b_1} + I_{d_1}), \quad (3)$$

$$I_{d_1} = I_{E_1} - (I_{a_1} + I_{b_1} + I_{c_1}), \quad (4)$$

where $I_{E_1} = I_{Batt_1} - I_{sys_1}$. Similarly, the current flow through other segments of the organism's power bus can be obtained.

In this simple configuration, the current flow between robot 1 and robot 2 can be obtained from the relation

$$I_{c_1} = I_{a_2}. \quad (5)$$

That is, the current flow through side-C of robot 1 is equivalent to the current flow through side-A of robot 2. Therefore

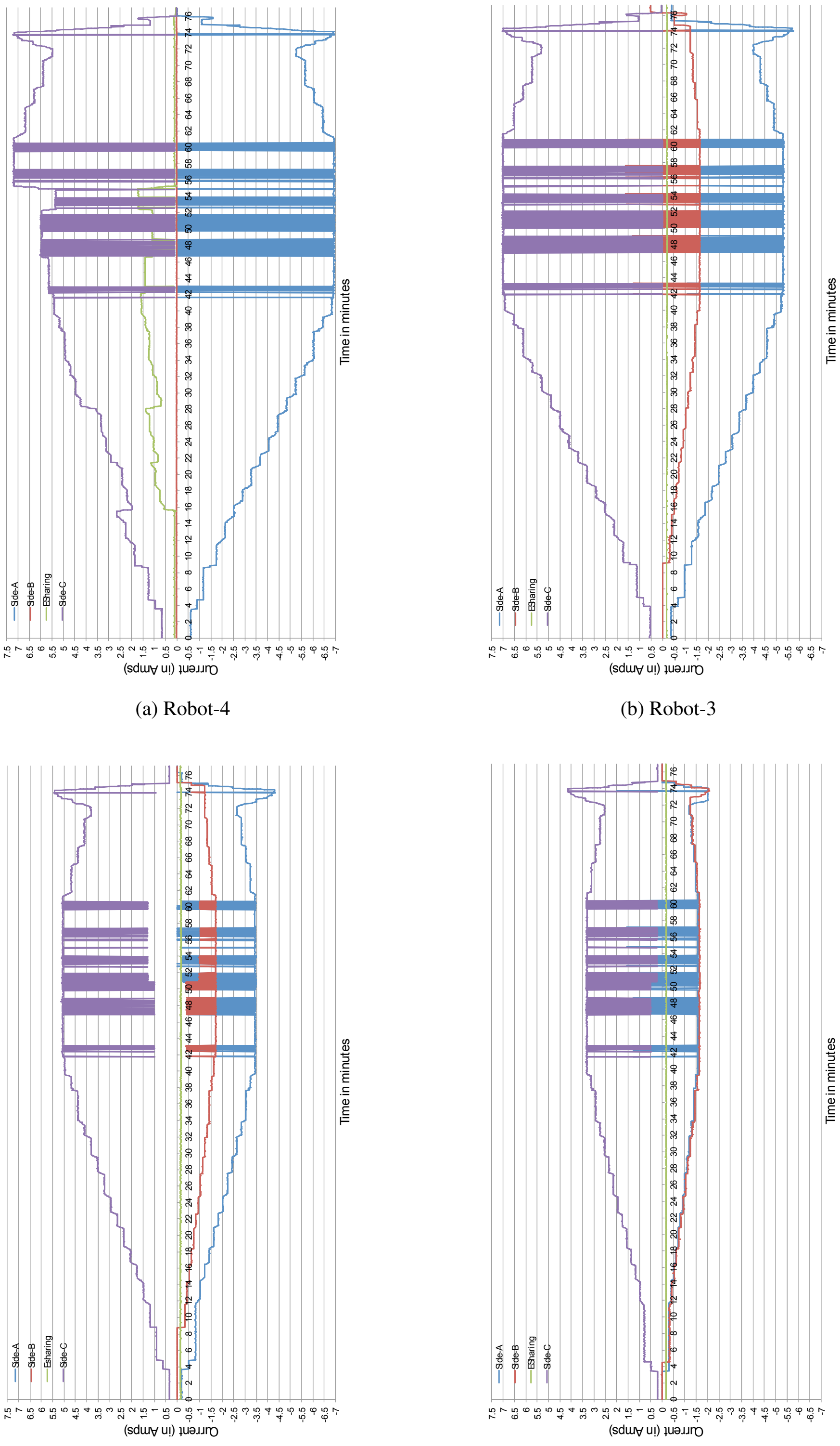

(a) Robot-4

(b) Robot-3

(c) Robot-2

(d) Robot-1

Figure 7: Power sharing in a REPLICATOR organism: the graph shows the current flow through each robotic module of the organism. Each graph shows the current flow through side A, B, C and the energy sharing module of a robot. The horizontal axis represents the time in minutes and the vertical axis represents the electrical current in amperes.

using the above relation,

$$\begin{aligned} I_{E_1} - I_{a_1} - I_{b_1} - I_{d_1} &= I_{E_2} - (I_{b_2} + I_{c_2} + I_{d_2}), \\ I_{E_1} - I_{E_2} &= -(I_{b_2} + I_{c_2} + I_{d_2}) + (I_{a_1} + I_{b_1} + I_{d_1}). \end{aligned} \tag{6}$$

Similarly, the current flow between side-C of robot 2 and side-A of robot 3 can be obtained from the equality $I_{c_2} = I_{a_3}$ as,

$$\begin{aligned} I_{E_2} - (I_{a_2} + I_{b_2} + I_{d_2}) &= I_{E_3} - (I_{b_3} + I_{c_3} + I_{d_3}), \\ I_{E_2} - I_{E_3} &= (I_{a_2} + I_{b_2} + I_{d_2}) - (I_{b_3} + I_{c_3} + I_{d_3}). \end{aligned} \tag{7}$$

and, finally the current flow between robot 3 and robot 4 is obtained as,

$$\begin{aligned} I_{E_3} - (I_{a_3} + I_{b_3} + I_{d_3}) &= I_{E_4} - (I_{b_4} + I_{c_4} + I_{d_4}), \\ I_{E_3} - I_{E_4} &= (I_{a_3} + I_{b_3} + I_{d_3}) - (I_{b_4} + I_{c_4} + I_{d_4}). \end{aligned} \tag{8}$$

The dynamic power sharing tests were performed to observe the individual and collective system behaviour – abilities and limitations, with the proposed power management system in different operating conditions. Such measurements will serve as the basis of application software development to control the distributed energy flow in more complex morphologies. In this regard, "robot-4" in the chain through its docking side-C was connected with an external power source that can deliver a continuous current of 8 Amps at 25 volts. In addition, an external power supply was also connected at the battery terminals of robot-4 that can deliver a maximum of 2 Amps of continuous current. "Robot-3" that was next in the chain connected with robot-4 through its side-C, has a single power source connected at its docking side-B. "Robot-2" that was connected with robot-3 through its side-A in the chain has again a single power source connected at its docking side-B. At the end, "Robot-1", i.e., last in the chain, has two power sources, connected at its docking side-B and-A, respectively. For a detailed analysis, the current flow measurements/readings at each robotic module from its docking interfaces and the energy sharing module were then stored on a PC connected with each robotic module over a UART interface.

To observe the collective system behaviour at different voltage levels, the voltage levels on the different power supplies were varied gradually with respect to each other to induce the variable current flow through the organism's power bus. The graphs in fig. 7a, 7b, 7c and 7d, show the current flow readings through sides A, B, C and the energy sharing module of Robot-4, Robot-3, Robot-2, and Robot-1, respectively. The horizontal axis represents the time in minutes and the vertical axis stands for the current in Amps. Positive current values in the graph indicate the current flow into the robot from the particular docking interface and vice versa.

The graph in the fig. 7a shows the current flow into the system though side-C of robot-4. By adjusting the voltage levels of the attached power supplies in the organism the energy sharing module at robot-4 starts energy sharing shortly before the minute 16th on the time scale. The current flow through side-B remained zero due to the absence of any source or sink. The current flow from the two power sources was then flowed through side-A of robot-4. At robot-3, according to fig. 7b current enters into the system through side-C. Due to the absence of a battery pack or a source at the battery terminals the current flow at energy sharing module remained negative. That is, the on-board system electronics was powered from the power bus current. Depending upon the voltage levels on the two sides, the inward current flow through side-C was then divided between the side-B and side-A of robot-3. At robot-2, fig. 7c shows the current flow through side-A,B,C and the energy sharing module. Again, due to the absence of a local power source – battery pack, the on-board system electronics was powered from the power bus. At the end, a similar behavior can be seen in fig. 7d of robot-1 in the organism.

The oscillations in the graphs were appeared due to the system's innate fault tolerance. To describe the system behavior during these oscillations on the organism's power bus, first consider the oscillations appeared shortly before the 42^{nd} minute – on the time axis, at robot-4 in fig. 7a. As soon as the current flow on side-A reached 7 amps the current limiter on the particular docking interface automatically turned down/shuts off. The oscillations then begun

as the particular current limiter tried to regain the previous/steady state with its auto-reset functionality. The effect of these oscillations then appeared successively as a chain reaction in the organism. For instance, during the same time instant, reactively the current flow through side-B of robot-3 becomes positive and the current flow through side-A was dropped to that amount – equivalent to the current flowing inward through side-B. Similarly, on robot-2 in fig. 7c the current flow on side-C was not dropped to zero rather it stayed at 1 amp. Likewise, the similar effect appeared on robot-1, as can be seen in fig. 7d. Another significant system behavior observed at energy sharing module of robot-3,-2, and robot-1 was that, the current flow through the energy sharing module remained consistent/uniform i.e., had no oscillations, through out the experiments. This particular system behavior ensures the steady state operations within the robotic modules that were energetically weak – dependent on other robotic modules, in an organism.

The energy sharing readings/measurements and the system innate fault tolerance in our simple organism structure provides us a robust platform that can be used to develop and explore the collective system – multi-robotic organism, behavior with energy sharing ability in more complex scenarios.

8. Simulation Framework

To further explore the advantages of dynamic power sharing in collaborative operations of autonomous robotic modules in an organism in the absence of sufficient number of REPLICATOR robotic modules, we had devised a simulation framework. The simulation framework called as, *Replicator Power Flow Simulator*, was developed in the light of experience gained with the real REPLICATOR robotic modules, as presented above. Our simulation framework consists of two parts: the front end and the simulation engine. The front-end was designed in LabWindows

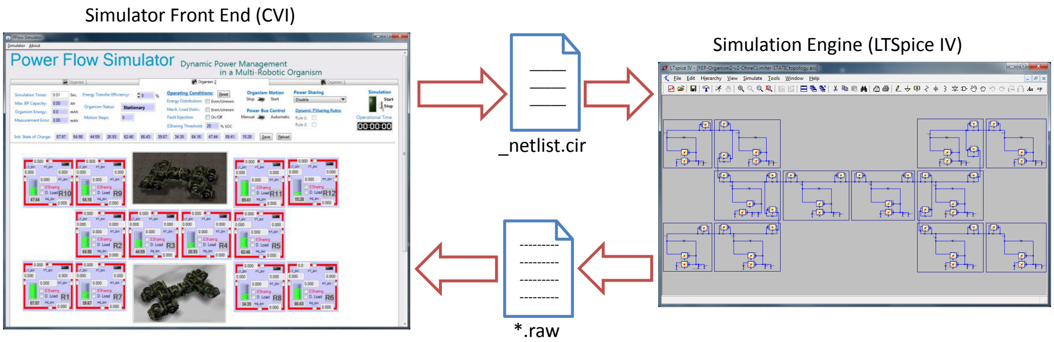

Figure 8: Simulation framework: REPLICATOR Power Flow Simulator

(CVI) and at the back-end a SPICE (simulation program with integrated circuit emphasis) simulator software from Linear technology (LT), i.e., LTSpcie IV, was integrated.

Fig. 8 shows the overview of the simulation framework. The front-end that was designed in LabWindow/CVI provides the graphical view of the whole organism from power management perspective. The particular graphical interface was especially designed to control and monitor the current flow through the segments of the organism's power bus, i.e., at docking interfaces and at the energy sharing module present in the power management system of each robotic module. In order to obtain more realistic power flow measurements in the organism, during run time, i.e., on each iteration, the simulation front-end generates a Spice netlist of the whole organism. The Spice netlist, i.e., *.cir file, contains the power management components with the configuration – their interconnection, that defines the power flow mechanism in the organism. The simulation engine was then invoked in DOS mode from the simulation front-end to process the netlist in background. The result of the simulation, i.e., current flow measurements at different points in the system, was then stored in ASCII format in a *.raw file. At the end, the simulation front-end read out the current flow measurements from the generated *.raw file to update the energetic status of the robotic modules in the organism and in the graphical interface.

Considering the complexity of the under lying system, at this development stage to gain more experience and to evaluate the operations of dynamic power management system in a multi-robotic organism, the REPLICATOR power flow simulator was developed for two types of organisms.

8.1. Power Sharing Mechanisms

Before describing the organisms structure, it is important to define the power sharing mechanisms/schemes that are now possible with the proposed power management system. And also, to evaluate their end effect in different operating conditions. This sub-section defines different variants of power sharing schemes for powering REPLICATOR multi-robotic organism especially devised to evaluate/observe their effect on longevity of the organism.

8.1.1. No Power Sharing:

This is the most obvious scenario, in which even though have the ability the robotic modules in the organism don't share their on-board energy reserve during their collective collaborative actions in the environment. The modules in this scenario coordinate with each other at the application layer such as, sharing sensory information, coordinating tasks, synchronizing movements, etc., but solely depend on their on-board energy reserve to meet their power demands.

Following are the effects that can be observed in a multi-robotic organism without power sharing.

- A major drawback of this topology appears when an energetically weaker robot in the organism ran out of energy and due to this the organism becomes unable to continue it's operations, e.g., movement, in the environment.
- In a similar scenario where the energetically weaker robot(s) in the organism due to energy deficiency becomes unable to detach (un-dock) itself from other modules in the organism or vice versa. In either case the whole organism becomes paralyzed – unable to function or move.

8.1.2. Power sharing without power flow control:

Also named as, *static power sharing* due to a single power bus in the organism for energy sharing. In this topology, the modules in the organism acquired the ability to share their on-board energy reserve with other modules without having control over the current flow through the organism's power bus. A single power bus is established between the autonomous modules of an organism for dynamic power sharing. The energy donor on the bus will always be the energetically stronger module(s) in the organism.

Following are the effects of the said topology that may appear on the operations of a multi-robotic organism:

- A major drawback of the said topology appears at energetically healthy robotic module(s) – energy donors, in the organism, as they quickly loose their on-board energy reserve. This phenomenon may induce high current flow through the organism's power bus depending upon the number of dependent robotic modules in the organism and the energy donors.
- In a faulty situation, for instance, a short circuit due to a mechanical or electronic failure in a robotic module, in worst case, since the modules don't have the control over the current flow through the organism's power bus, the whole system may collapse – the whole electronic circuitry may gets damage or burnout.

8.1.3. Power sharing with power flow control:

Can also be categorized as proactive power management. Using this strategy the modules in the organism now has the ability to dynamically control the direction of current flow flowing through the organism's power bus. This means the autonomous modules in the organism can form more than one or sub power buses as required.

- With the dynamic control over the organism's power bus, the modules in the organism are able to isolate the system malfunctions or abrupt failures, e.g., short circuit, or a malfunctioning component in a module. This way, an organism can still continue its autonomous operations even in the presence of malfunctioning robotic modules.

For dynamic power sharing with power flow control in a multi-robotic organism, we have devised two simple power sharing strategies. These strategies allow the modules to form dynamic sub-power buses in the organism with the information about the state of charge of neighbouring modules in the organism.

- ***Rule 1:***
  It is based on the *local energy distribution* information available to each robotic module. In this topology, every module in the organism creates a *local energy distribution table* that includes it's state of charge (SOC) and SOC of it's direct neighbours on the four docking sides. The local energy distribution table entries are then updated on every iteration – every second. An energetically healthy robot, i.e., having SOC > energy sharing threshold, shares its on-board energy reserve by opening the current flow path in the particular direction if anyone among its direct neighbour's SOC was less than the energy sharing threshold. Table 4 shows the local energy distribution table that keeps record of SOC of each robot and its direct neighbours in the organism.

Table 4: Local energy distribution graph with rule 1 power sharing scheme

Itself	Front neighbour	Right neighbour	Rear neighbour	Left neighbour
SOC_{robotX}	$SOC_{robotX+1}$	$SOC_{robotX+2}$	$SOC_{robotX+3}$	$SOC_{robotX+4}$

- ***Rule 2:***
  It is based on *global energy distribution* information gathered by each module in the organism. With this power sharing strategy, each robot in the organism maintains a global energy distribution table that not only lists its direct neighbours but also their direct neighbours as well. Therefore, in this topology an energetically healthy robot shares its on-board energy reserve if anyone from its direct neighbours or their direct neighbours has SOC less than the energy sharing threshold. The power bus is then established between the energy donor and the acceptor robot by closing the electronic switches in the particular path. Table 5 shows the global energy distribution table maintained at each robotic module in the organism.

Table 5: Global energy distribution graph with rule 2 power sharing scheme

	Front neighbour	Right neighbour	Rear neighbour	Left neighbour
SOC_{robotX}	$SOC_{robotX+1}$	$SOC_{robotX+2}$	$SOC_{robotX+3}$	$SOC_{robotX+4}$
$SOC_{robotX+3}$	SOC_{robotX}	$SOC_{robotX+11}$	$SOC_{robotX+12}$	$SOC_{robotX+13}$
$SOC_{robotX+4}$	$SOC_{robotX+16}$	SOC_{robotX}	$SOC_{robotX+14}$	$SOC_{robotX+15}$
$SOC_{robotX+1}$	$SOC_{robotX+6}$	$SOC_{robotX+7}$	SOC_{robotX}	$SOC_{robotX+5}$
$SOC_{robotX+2}$	$SOC_{robotX+8}$	$SOC_{robotX+9}$	$SOC_{robotX+10}$	SOC_{robotX}

8.2. System Power Consumption Model

Our system power consumption model includes two types of loads, namely the *static* and *dynamic load*. The term *static load* refers to the power consumption of essential system components that include core processing unit, peripheral controllers, power management module, and other essential sensing components, that are necessary to keep a robotic module alive. Whereas, the term *dynamic load* refers to the power consumption of actuators – 2D and 3D drive and their controllers, that are necessary for a module to locomote on different surfaces. They are considered as dynamic system load, since they do not required to be ON all the times during the normal operations of a robotic module and consume more power compared to the power consumption of essential system components.

For the sake of simplicity, without considering the complex kinematics involved in the organism motion, the dynamic load calculation uses the power consumption of a hinge (3D) drive present on a REPLICATOR backbone robot. Under different load conditions in the organism the power consumption of a hinge (3D) drive can be determined from the torque required to lift the n number of robotic modules, i.e.,

$$\begin{aligned} \tau &= (\sum_{i=1}^{n} i) \cdot F \cdot d \\ &= \frac{n(n+1) \cdot mg \cdot d}{2} \end{aligned} \tag{9}$$

where, the average weight of a REPLICATOR robot is roughly 1 kg, the gravity "g" is 9.8 m/s^2, and the variable "d" is the distance that is moved up from pivot point.

The torque required by the actuator motor itself "τ_r" can be calculated as,

$$\tau_r = \frac{\tau}{r_r \cdot \eta} \tag{10}$$

where, the gear reduction ratio of the hinge drive is 800 : 1, and the efficiency "η" is roughly around 75%. The amount of current required "i_r" with "τ_r" can be therefore obtained as,

$$I_r = \frac{\tau_r}{\tau c} + i_0, \tag{11}$$

where, "τ_c" is the torque constant of the brushless DC motor, i.e., Portescap 32BF, and equals to 7.8 mNm. The current consumption of the motor drive without load "i_0" is 65 mA at 12 V.

The motor speed required for the desired actuation "v_r" is then obtained as,

$$v_r = v \cdot r_r \tag{12}$$

where, "v" is the nominal motor speed and "r_r" is the reduction ratio, as mentioned in eq. 10. The amount of voltage required to run the motor at a desired speed "v_r" can thus obtained as,

$$V_r = \frac{v_r}{s_c} \tag{13}$$

where, s_c is the speed constant of the brushless DC motor. Based on the above calculations the power consumption "P" of the actuator motor can now be obtained as,

$$P = V_r \cdot I_r. \tag{14}$$

8.3. Organism 1

To model a relatively simple scenario with the experience gained while experimenting with the REPLICATOR hardware, we had chosen a REPLICATOR organism consisting of six Backbone robotic modules docked to each other in the form of a chain. Fig. 9 shows the REPLICATOR multi-robotic organism of type 1 consisting of six REPLICATOR backbone robotic modules, constructed in Symbricator Robot 3D simulator [21]. Fig. 9a shows an organism moving on a flat surface exhibiting a sinusoidal movement pattern, whereas, in figure 9b the organism is shown as crossing an obstacle on an uneven surface.

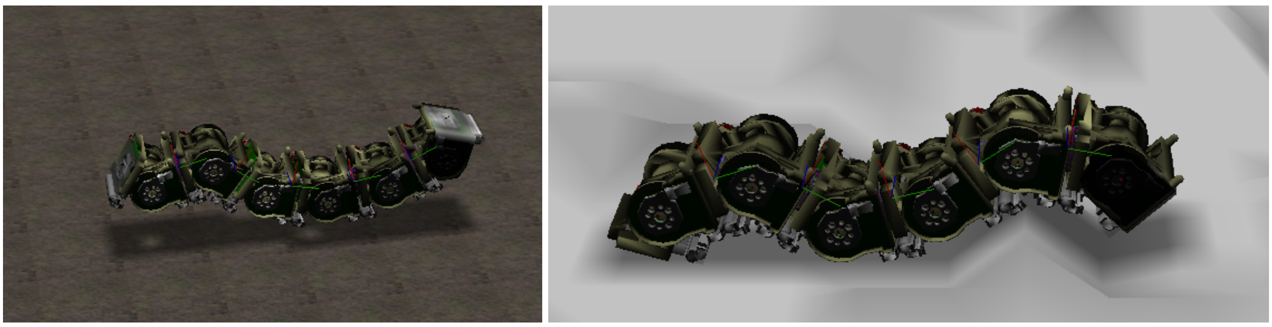

(a) (b)

Figure 9: REPLICATOR Multi-robotic organism of type 1 consisting of 6 REPLICATOR backbone robotic modules in a snake like structure in Symbricator Robot 3D simulator [21]: (a) Organism while moving on a flat surface, (b) similar organism while crossing an obstacle on an uneven surface.

8.3.1. Motion Model

In order to simulate the dynamic current flow through the organism's power bus between the robotic modules, a simple motion model that is based on sinusoidal movement of the robotic modules was devised. On each step, the motion dynamics – the coordinated movement of robotic modules in a particular pattern, of the organism was used to create the dynamic power demand at each robotic module in the organism. Based on the active power sharing rule/strategy the calculated power was then taken/consumed from the respective robotic module's or the donor robot's battery pack.

Since it is quite complex and difficult to mathematically model the motion dynamics of such a multi-robotic organism that involves multiple degrees of freedom, therefore for the sake of simplicity we have used the matrix notation to define the motion pattern of the robotic modules in the organism. The particular motion model uses the 3D hinge on each robotic module to model the motion pattern of the organism. To generate the sinusoidal motion pattern in the organism for its locomotion, on each step the motion model matrix defines the state of hinge drive at each module, i.e., upward, downward or no movement.

$$MM_{Org1} = \begin{bmatrix} 0 & 0 & 0 & 0 & 0 & 0 \\ 1 & 2 & 0 & 0 & 0 & 0 \\ 0 & 0 & 3 & 0 & 0 & 0 \\ 0 & -1 & 0 & 0 & 0 & 0 \\ -1 & 2 & 0 & 0 & 0 & 0 \\ 0 & 0 & 0 & 3 & 0 & 0 \\ 0 & 0 & 0 & -2 & 0 & 0 \\ 0 & -1 & 2 & 0 & 0 & 0 \\ 1 & 0 & 0 & 0 & 2 & 0 \\ 0 & 0 & 0 & -2 & 0 & 0 \\ 0 & 2 & -1 & 3 & 0 & 0 \\ 0 & -2 & 0 & 0 & 0 & 1 \\ -1 & 2 & 0 & 0 & -2 & 0 \\ 0 & 0 & 3 & -1 & 2 & 0 \\ 0 & 0 & 0 & 3 & 0 & -1 \\ 0 & 0 & -1 & 0 & -2 & 0 \\ 0 & -1 & 3 & 0 & 0 & 0 \end{bmatrix}$$

The motion matrix (MM_{Org1}) shows the modeled movement pattern of the robotic modules in organism 1. Where, "0" in the matrix denotes "no motion", a positive value denotes the motion in upward direction from pivot position and a negative value denotes the backward movement – back to the pivot position. The numbers in the column represent the number of modules that has to be lifted upward or downward by the particular module in the organism to achieve a particular movement pattern on each step. Further, each row in motion matrix (MM_{Org1}) corresponds to a motion step.

8.3.2. Experiments

In the experiments, we have used two significantly important factors to evaluate the effectiveness of our devised power management system that include, initial energy distribution among the robotic modules and the mechanical load associated with the motion of the organism on a particular terrain.

Table 6 shows the test scenarios devised for the organism with respect to the energy and mechanical load distribution among the robotic modules. That is, case C_1 initializes the robotic modules with even energy distribution and uses even mechanical load during the motion. Thus simulating a scenario in which all the modules of an organism are energetically equal or equally charged. To simulate a scenario in which the robotic modules autonomously form an organism in the arena with different energetic states, case C_2 initializes the organism with uneven energy distribution among the modules but due to the sinusoidal movement pattern uses even mechanical load distribution during the collective locomotion.

For even and uneven energy distribution between the robotic modules we have randomly chosen three different topologies of organism 1. Fig. 10 shows the different energy distribution topologies of organism 1. Fig. 10a shows an

Table 6: Organism 1: experiment scenarios based on initial energy and the mechanical load distribution among the robotic modules

Case	Energy distribution	Mech. load distribution
C_1	*Even*	*Even*
C_2	*Uneven*	*Even*

even energy distribution between the robotic modules. Fig. 10b and 10c shows the randomly chosen uneven energy distribution between the robotic modules. Whereas, each box represents a robotic module and the numerical value in

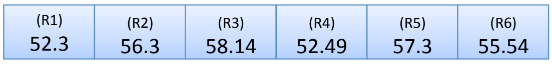

(a) Topology 1: even energy distribution in organism 1

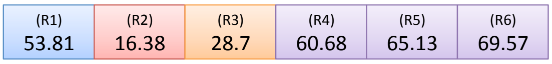

(b) Topology 2: uneven energy distribution in organism 1

(c) Topology 3: uneven energy distribution in organism 1

Figure 10: Energy distribution among the REPLICATOR robotic modules in organism 1. The numerical values in the boxes represent the state of charge of the particular robot in the organism. The color scheme i.e.,Green when > 80%, Violet when > 60%, Blue when > 40%, Orange when > 20%, and red when > 10%, depicts the different levels of state of charge of the particular robot.

it represent the state of charge of a particular robot in the organism.

In our simulation experiments we have chosen the system dependent parameters form the empirical results obtained with the real REPLICATOR robotic modules. It includes, maximum battery pack charge capacity of a REPLICATOR robot that was chosen as 1400 mAh, system static power consumption as 200 mA, and the dynamic power consumption values – 3D hinge drive, were obtained from the system power consumption model, as described in subsection 8.2. To lift the load of a robotic module a robotic module consumes 150 mA of current at nominal voltage, for a load of two robotic modules it consumes 294 mA, for three it consumes 806 mA, and for a load of four robotic modules its current consumption was 1575 mA at nominal system voltage.

To simulate collective locomotion, on each time step the organism motion model matrix entries – in each row, were used to assign the dynamic load to each module in the organism. A motion step was incremented when the organism successfully completed a motion pattern – a complete sinusoid. The organism motion stops as soon as the state of charge of any robotic module was dropped down to 10% of the max. battery pack capacity, i.e., $SOC(t) = 10\%SOC_{max}$.

Fig. 11 shows the current flow reading through the energy sharing module of each robot in organism 1 in different configurations. The positive values in the plots show the current flowing into the system and vice versa. The horizontal axis in the plots shows the time in seconds and the vertical axis shows the current in amperes. Before discussing the results visible in Fig. 11 it is important to consider the overall organism operational time and the covered motion steps. Table 7 shows the operational time of organism 1 in different scenarios. And, Table 8 shows the covered motion steps by organism 1. In an ideal scenario, i.e., having no abrupt system failures, in case C_1 and topology 1 – with even energy and mechanical load distribution, with *static* energy sharing scheme the organism 1 was able to move 179 motion steps and with *rule 1* it had moved 174 motion steps. Along with these readings now consider the measurements shown in fig. 11b. The oscillations at the energy sharing module with *static* energy sharing scheme show the robotic modules always share their energy even when all the modules were energetically healthy. In a real mobile organism such oscillations may case unwanted problems such as, resetting on-board electronics, unwanted noise in some sensor readings, etc. Whereas, with *rule 1* power sharing mechanism the robotic modules shared their energy only when they are required to.

In case C_2 and topology 2 – uneven energy distribution and even mechanical load distribution, the organism had covered with *static* energy sharing scheme 134 motion steps and with *rule 1* it had moved 145 motion steps. Depending upon the initial energy distribution the results in fig. 11b provides an evident of efficiently energy utilization with *rule 1*

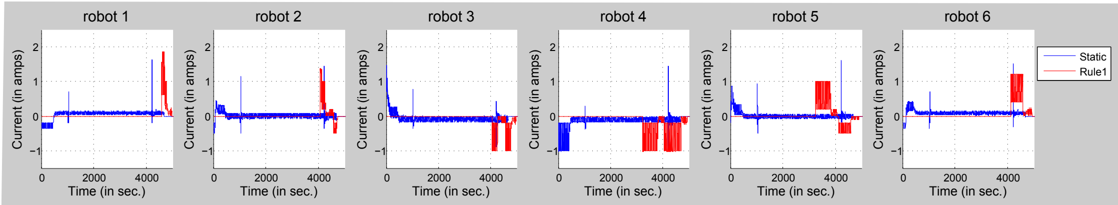

(a) Case C_1 and Topology 1

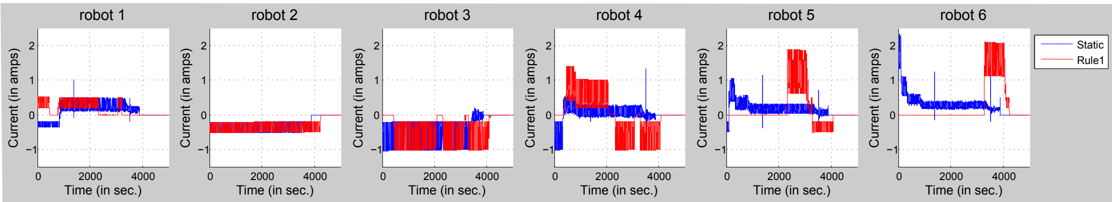

(b) Case C_2 and Topology 2

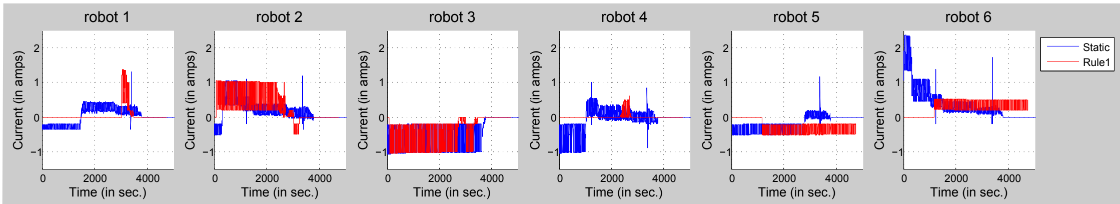

(c) Case C_2 and Topology 3

Figure 11: The current flow through the energy sharing module of each robot in organism 1 in different configurations. The positive values in the plots show the current flowing into the system and vice versa. The horizontal axis in the plots shows the time in seconds and the vertical axis shows the current in amperes. Each graph shows the measurements of *static* energy sharing in blue, and *rule* 1 in red.

Table 7: Operational time of organism 1 in different scenarios

	Case C_1	Case C_2	
Energy Sharing Rule	Topology 1	Topology 2	Topology 3
Static	01:51:22	01:24:17	01:34:49
Rule 1	01:48:08	01:30:02	01:21:18

Table 8: Motion steps covered by organism 1

	Case C_1	Case C_2	
Energy Sharing Rule	Topology 1	Topology 2	Topology 3
Static	179	135	152
Rule 1	174	145	130

energy sharing mechanism. In the last scenario, with case C_2 and topology 3, the organism has covered with *static* energy sharing scheme 152 motion steps and with *rule 1* it was able to move 130 motion steps. For a meaningful analysis of this scenario, again it is important to consider the initial energy distribution in the organism and the plots in fig. 11c. In this particular scenario, with *rule 1* energy sharing mechanism robot-2 shared its energy with robot-3, since its direct neighbour was energetically weak. Whereas, robot-4 did not shared its energy with robot-3 when robot-4 and robot-2 were energetically equal, as in case of *static* energy sharing mechanism. Hence, in the particular topology with *rule 1* the organism's distributed energy was not efficiently utilized. Here in this scenario, we can obtain

better or equivalent results by applying *rule 2* energy sharing mechanism.

A detailed analysis of the initial energy distribution in the later two topologies – topology 2 and 3, further explain the system behavior. Consider the uneven energy distribution topology-2 the right half of the organism – r4,r5 and r6, was energetically healthy whereas the left half of the organism – r1,r2 and r3, was energetically weak. In such a configuration *rule*-1 energy sharing scheme had better utilized the available energy in the organism by covering more motion steps compared to the *static* energy distribution scheme. In uneven energy distribution topology-3, the energetically healthier robotic modules – r2 and r6, were apart from each other. Therefore, *rule*-1 energy sharing scheme in such a configuration did not produce comparable results.

8.4. Organism 2

For our next set of experiments we had chosen an organism that was of relatively complex structure compared with organism 1. It consists of twice the number of robotic modules as in organism 1. Fig. 12 (a) and (b) show the REPLICATOR multi-robotic organism composed of twelve backbone robotic modules that were arranged in the form of a car with four limbs (actuator arms) and a central backbone like structure. The organism structure was also constructed in Symbricator Robot 3D simulator [21].

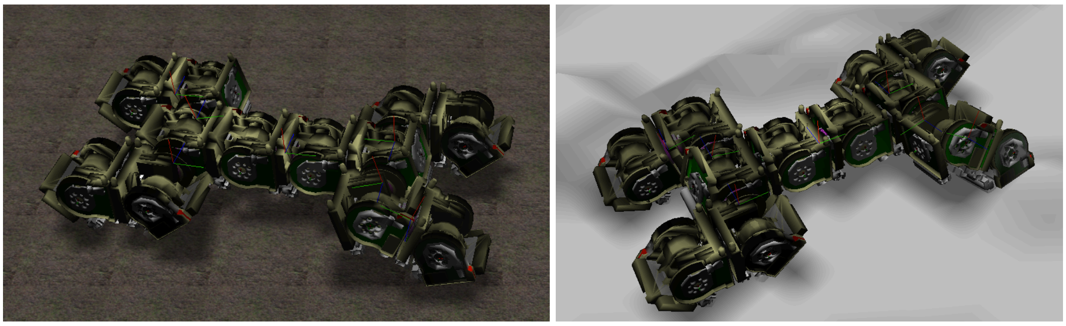

(a) (b)

Figure 12: REPLICATOR Multi-robotic organism of type 2: a REPLICATOR multi-robotic organism consisting of twelve backbone robotic modules arranged in the form of a car with four limbs (actuator arms) and a central backbone like structure moving on a flat surface. Organism 2 (a) moving on a flat surface and (b) while moving on a rough terrain. The organism structure was constructed in Symbricator Robot 3D simulator [21]

8.4.1. Motion Model

Similarly, a motion model for organism 2 was developed to simulate the coordinated movement of modules for locomoting themselves collectively form one place to the other in the arena. The motion model / movement pattern of the modules apply variable load to them which was then translated into electrical load. The electrical load was then deducted either from the on-board energy source or depending upon the active energy sharing scheme taken from the donor robot's battery pack.

The increased structural complexity of the multi-robotic organism also increased the available degrees of freedom and thus made it difficult to mathematically model even a simple movement pattern. Since it is not the scope of our work, therefore, we had devised a simple movement pattern of the robotic modules in the organism to simulate the dynamic current flow through the organism's power bus. As in case of organism 1, our motion model used the matrix notation to define the coordinated movement of the robotic modules in a particular fashion. The organism 2 motion model consisted of 12 motion steps that turn by turn actuated the respective robotic modules in the organism to achieve a certain movement pattern.

Matrices MM_{Org2_Step1} ... MM_{Org2_Step12} show the motion matrices defining the movement pattern of the robotic modules in organism 2 at each step. Where, "ϕ" in the motion matrices denotes "no motion", dash "–" denotes the absence of a robotic module in the particular position in the organism structure, "1" denotes the movement of the 3D hinge drive in upward direction from center position and "-1" denotes the downward movement of the 3D hinge drive.

For the sake of diversity in the simulation experiments, concerning mechanical load that appears at the robotic modules during collective locomotion, we have tried to model the mechanical load distribution in organism 2 in two different scenarios. The two scenarios include locomotion on a flat surface and on a uneven/rough terrain, as shown in fig. 12a and 12b. The locomotion on a flat surface was modeled with even load distribution among the four limbs of the organism 2. Whereas the locomotion of robotic module on a rough terrain was envisage with uneven load distribution among the four limbs of organism 2.

$$MM_{Org2\_Step1} = \begin{bmatrix} 1 & \phi & - & - & \phi & \phi \\ - & \phi & \phi & \phi & \phi & - \\ 1 & \phi & - & - & \phi & \phi \end{bmatrix}, \quad MM_{Org2\_Step2} = \begin{bmatrix} \phi & 1 & - & - & \phi & \phi \\ - & \phi & \phi & \phi & \phi & - \\ \phi & 1 & - & - & \phi & \phi \end{bmatrix},$$

$$MM_{Org2\_Step3} = \begin{bmatrix} \phi & \phi & - & - & \phi & \phi \\ - & \phi & 1 & \phi & \phi & - \\ \phi & \phi & - & - & \phi & \phi \end{bmatrix}, \quad MM_{Org2\_Step4} = \begin{bmatrix} \phi & \phi & - & - & \phi & \phi \\ - & \phi & \phi & 1 & \phi & - \\ \phi & \phi & - & - & \phi & \phi \end{bmatrix},$$

$$MM_{Org2\_Step5} = \begin{bmatrix} \phi & \phi & - & - & 1 & \phi \\ - & \phi & \phi & \phi & \phi & - \\ \phi & \phi & - & - & 1 & \phi \end{bmatrix}, \quad MM_{Org2\_Step6} = \begin{bmatrix} \phi & \phi & - & - & \phi & 1 \\ - & \phi & \phi & \phi & \phi & - \\ \phi & \phi & - & - & \phi & 1 \end{bmatrix},$$

$$MM_{Org2\_Step7} = \begin{bmatrix} -1 & \phi & - & - & \phi & \phi \\ - & \phi & \phi & \phi & \phi & - \\ -1 & \phi & - & - & \phi & \phi \end{bmatrix}, \quad MM_{Org2\_Step8} = \begin{bmatrix} \phi & -1 & - & - & \phi & \phi \\ - & \phi & \phi & \phi & \phi & - \\ \phi & -1 & - & - & \phi & \phi \end{bmatrix},$$

$$MM_{Org2\_Step9} = \begin{bmatrix} \phi & \phi & - & - & \phi & \phi \\ - & \phi & -1 & \phi & \phi & - \\ \phi & \phi & - & - & \phi & \phi \end{bmatrix}, \quad MM_{Org2\_Step10} = \begin{bmatrix} \phi & \phi & - & - & \phi & \phi \\ - & \phi & \phi & -1 & \phi & - \\ \phi & \phi & - & - & \phi & \phi \end{bmatrix},$$

$$MM_{Org2\_Step11} = \begin{bmatrix} \phi & \phi & - & - & -1 & \phi \\ - & \phi & \phi & \phi & \phi & - \\ \phi & \phi & - & - & -1 & \phi \end{bmatrix}, \quad MM_{Org2\_Step12} = \begin{bmatrix} \phi & \phi & - & - & \phi & -1 \\ - & \phi & \phi & \phi & \phi & - \\ \phi & \phi & - & - & \phi & -1 \end{bmatrix}$$

For locomotion on a flat surface, the load matrix $LM_{Org2\_Even\_lifting}$ defines the even distribution of mechanical load among the robotic modules in organism 2 during their erection phase – when modules were lifting themselves from ground for a particular move. Following the sinusoidal pattern to complete one motion cycle, in the next step the modules in the organism lower themselves in a particular position. For this purpose, the load matrix $LM_{Org2\_lowering}$ define the associated mechanical load at each robotic module in the organism. Our motion model uses the load matrix $LM_{Org2\_Even\_lifting}$ during the motion steps MM_{Org2_Step1} to MM_{Org2_Step6} to obtain the associated load at each robotic individual in the organism. And, the load matrix $LM_{Org2\_lowering}$ was used during the motion steps MM_{Org2_Step7} ... MM_{Org2_Step12} to obtain the associated load at each robotic individual in the organism.

$$LM_{Org2\_Even\_lifting} = \begin{bmatrix} 3 & 2 & 0 & 0 & 2 & 3 \\ 0 & 0 & 3 & 3 & 0 & 0 \\ 3 & 2 & 0 & 0 & 2 & 3 \end{bmatrix}, \quad LM_{Org2\_lowering} = \begin{bmatrix} 1 & 1 & 0 & 0 & 1 & 1 \\ 0 & 0 & 1 & 1 & 0 & 0 \\ 1 & 1 & 0 & 0 & 1 & 1 \end{bmatrix}$$

Similarly, for locomotion on a rough terrain – with crust and troughs, the load matrix $LM_{Org2\_Uneven\_lifting}$ defines the uneven mechanical load distribution among the modules of organism 2 during the erection phase, i.e.,

$$LM_{Org2\_Uneven\_lifting} = \begin{bmatrix} 3 & 2 & 0 & 0 & 3 & 4 \\ 0 & 0 & 3 & 4 & 0 & 0 \\ 4 & 3 & 0 & 0 & 2 & 3 \end{bmatrix}.$$

And likewise, the motion model uses the load matrix $LM_{Org2\_Uneven\_lifting}$ during the motion steps MM_{Org2_Step1} to MM_{Org2_Step6} to obtain the associated load at each robotic individual in the organism. And, the load matrix $LM_{Org2\_lowering}$ was used during the motion steps MM_{Org2_Step7} ... MM_{Org2_Step12} to obtain the associated load at each robotic individual in the organism.

8.4.2. Experiments

Similarly, based on initial energy distribution and the mechanical load associated with the collective locomotion of robotic modules in the organism, we have evaluated/compared the effects of dynamic power sharing in a multi-robotic organism in different conditions within the simulated environment. Table 9 shows the test scenarios devised for organism 2 with respect to the energy and mechanical load distribution among the robotic modules. Case C_1 uses even energy and mechanical load distribution, C_2 uses even energy but uneven mechanical load distribution, C_3 uses uneven energy but even mechanical load distribution, and at the end, C_4 uses uneven energy and mechanical load distribution among the docked robotic modules.

Table 9: Experiment scenarios based on initial energy and the mechanical load distribution between the robotic modules of organism 2

Case	Energy distribution	Mech. load distribution
C_1	*Even*	*Even*
C_2	*Even*	*Uneven*
C_3	*Uneven*	*Even*
C_4	*Uneven*	*Uneven*

For even and uneven energy distribution experiments, we have randomly chosen an even and two uneven energy distribution topologies for organism 2. Fig. 13 shows three energy distribution topologies for organism 2. The numerical values at each robotic module – in the boxes, represent the state of charge of the particular robot in the organism. Fig. 13a shows the even distribution among the robotic modules as if an organism had detached itself from a recharge station. Fig. 13b shows an uneven energy distribution topology randomly chosen for organism 2. In the particular topology, the energetically stronger modules – r1 and r11, were placed in separate actuator arms. A energetically weaker module – r12, was docked with r11 in one of the actuator arm. Fig. 13c shows another uneven energy distribution topology to evaluate the influence of initial energy distribution on the operations of multi-robotic organism.

Likewise, the power flow simulator on every simulation instance used motion model and the associated load matrices to simulate the organism locomotion. Table 10 shows the operational time of organism 2 in different scenarios during simulation runs. And, table 11 shows the covered simulated motion steps by organism 2. To describe the results shown in the two tables 10, 11 in a more meaningful manner it is important to consider the initial energy distribution in the organism and the energy sharing among the robotic modules during the simulation runs.

Table 10: Operational time of organism 2 in different scenarios during simulation runs

E. Sharing /	Case C_1	Case C_2	Case C_3		Case C_4	
E. dist. schemes	Topology 1	Topology 1	Topology 2	Topology 3	Topology 2	Topology 3
Static	2:30:08	2:13:09	01:54:58	2:16:12	1:43:04	2:07:21
Rule 1	2:24:48	2:09:39	01:50:01	2:21:53	1:35:01	2:04:08
Rule 2	2:25:06	2:08:48	01:51:37	2:22:01	1:41:57	2:03:47

Table 11: Covered motion steps by organism 2 during simulation

E. Sharing /	Case C_1	Case C_2	Case C_3		Case C_4	
E. dist. schemes	Topology 1	Topology 1	Topology 2	Topology 3	Topology 2	Topology 3
Static	182	161	140	165	125	154
Rule 1	175	156	135	171	115	150
Rule 2	177	155	136	172	124	149

First of all, analyzing the system behavior in case C_1 and energy distribution topology 1. Fig. 14 shows the energy sharing among the robotic modules of organism 2 measured at the power management energy sharing module with

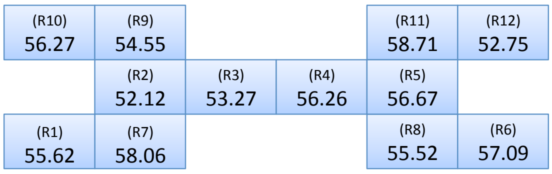

(a) Topology 1: even energy distribution

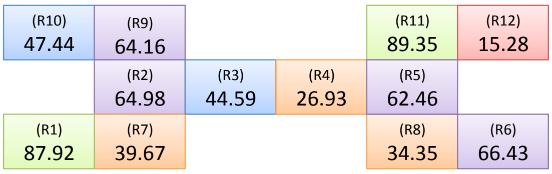

(b) Topology 2: uneven energy distribution

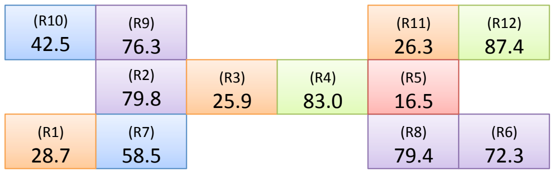

(c) Topology 3: uneven energy distribution

Figure 13: Energy distribution among the REPLICATOR robotic modules in organism 2. The numerical values in the boxes represent the state of charge of the particular robot in the organism. The color scheme i.e., Green when > 80%, Violet when > 60%, Blue when > 40%, Orange when > 20%, and red when > 10%, depicts the different levels of state of charge of a robot.

configuration C_1 and topology 1. The positive current values in the plots show the current flow into the system and vice versa. The horizontal axis shows the time scale in seconds and the vertical axis stands for current in amps. In this scenario, the organism 2 was able to cover 182 motion steps in case of *static* energy sharing scheme, 175 motion steps in case of *rule* 1 energy sharing and 177 motion steps in case of *rule* 2 energy sharing mechanism.

In regards to the covered motion steps it is evident that the static energy sharing resulted better. As we described the system complexities while analyzing the energy sharing plots of organism 1, with *static* energy sharing the modules in the organism 2 had shared their energy with each other all the times. This means, the on-board battery packs of individual robotic modules in the organism were connected in parallel. In this parallel connection of battery packs, the pack with higher voltage will be discharged first and then successively the rest of the battery packs. This discharging of multiple-battery packs in parallel irrespective of their locality in the organism create oscillations at the energy sharing module of each robot. These oscillations – inward or outward flow of current from the system, defines the energetic status i.e., energy donor or acceptor, of a robotic module with respect to other robotic modules in the organism. After a detailed analysis of a robot's behavior from the energy sharing plots shown in fig. 14, even though the whole system is operating in a steady state, the continuous oscillations on the organism's power bus during collective locomotion may result in unwanted system errors e.g., resetting controllers, noise in sensor measurements, etc. The oscillations show that at one time instant a particular robotic module, e.g., robot 1, was energy "donor" and in the next time instant it became energy "acceptor" / dependent in the organism. To further analyze the system behavior form the perspective of energy losses during the three energy sharing mechanisms, we had compiled the results that show the energy losses during energy sharing in the organism. Fig. 20a shows the current losses measured as the difference between the energy donated and accepted in the organism during the three energy sharing schemes. The measurements of *static* energy sharing in blue, *rule* 1 in black and *rule* 2 in magenta. The horizontal axis shows the time scale in seconds and the vertical axis stands for current in mA. The current losses during *static* energy sharing roughly oscillates between 13 mA and 20 mA. Where as, with *rule* 1 and *rule* 2 energy sharing the current losses was minimal.

Fig. 15 shows the energy sharing among the robotic modules of organism 2 measured at the power management energy sharing module with configuration C_2 and topology 1. The positive current values show the current flow into the system and vice versa. The organism in this scenario had covered 161 motion steps with *static* energy sharing, 156 motion steps with *rule* 1, and 155 motion steps with *rule* 2 energy sharing scheme. Due to uneven mechanical load distribution, the organism had covered fewer motion steps compared to the case C_1. Although with *static* energy sharing the organism had covered more motion steps but with *rule* 1 and *rule* 2 energy sharing, the energy reserve of the robotic modules remained conserved and only utilized when desired. Fig. 20b shows the current losses measured as the difference between the energy donated and accepted in the organism during the three energy sharing schemes.

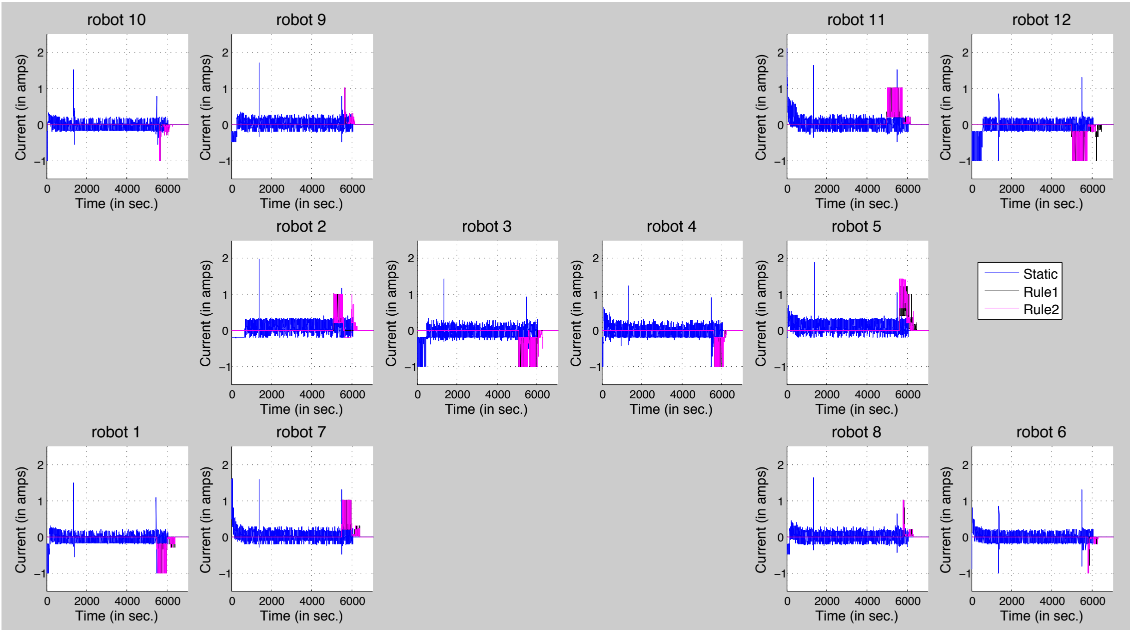

Figure 14: Energy sharing among the robotic modules of organism 2 measured at the power management energy sharing module with configuration C_1 and topology 1. The positive current values show the current flow into the system and vice versa. The horizontal axis shows the time scale in seconds and the vertical axis stands for current in amps. Each graph shows the measurements of *static* energy sharing in blue, *rule* 1 in black and *rule* 2 in magenta.

Likewise, the current losses with *rule* 1 and *rule* 2 energy sharing remained minimal.

So far we have observed the collective system behavior in even energy distribution topology in combination with even and uneven mechanical load distribution scenarios. Now to observe and analyze collective system behavior in uneven energy distribution scenario, fig. 16 shows the energy sharing among the robotic modules of organism 2 measured at the power management energy sharing module with configuration C_3 and topology 2. The positive current values show the current flow into the system and vice versa. The organism in this scenario had covered 140 motion steps with *static* energy sharing, 135 motion steps with *rule* 1, and 136 motion steps with *rule* 2 energy sharing scheme. For a detailed analysis of the collective system behavior during the simulation run it is important to consider the initial energy distribution in the organism, as it defines the energy – current, flow through the organism's power bus. In topology 2, with *static* energy sharing scheme the energetically stronger robotic modules r1 and r11 become the energy donor for the rest of the robotic modules in the organism. Whereas, with *rule* 1 and *rule* 2 energy sharing scheme the robotic modules in the organism form sub-power buses. This way the energy reserve of robotic modules remain conserved in the organism. Fig. shows the current losses during energy sharing in the three energy sharing schemes. The current losses during *static* energy sharing scheme varied roughly between 10 mA and 24 mA at nominal system voltage. Whereas, in *rule* 1 and *rule* 2 energy sharing scheme, due to local energy sharing the current losses between the robotic modules remained minimum.

Again to analyze the system behavior in an uneven energy distribution, we had ran the organism 2 simulation using topology 3 as the initial energy distribution among the robotic modules. Fig. 17 shows energy sharing among the robotic modules of organism 2 measured at the power management energy sharing module with configuration C_3 and topology-3. The organism in this scenario had covered 165 motion steps with *static* energy sharing, 171 motion steps with *rule* 1, and 172 motion steps with *rule* 2 energy sharing scheme. Interestingly, in the particular scenario with *static* energy sharing scheme, the organism had covered fewer motion steps compared to *rule* 2 energy sharing scheme. From the energy sharing plots in fig. 17, evidently the energy is shared locally e.g., between robot r1 and r7, r9 and r10, r3 and r4, and r11 and r12. Fig. 20d shows the current losses between the robotic modules in case C_3 and topology-3. In this case, again the current losses during *static* energy sharing scheme varied roughly between 10 mA

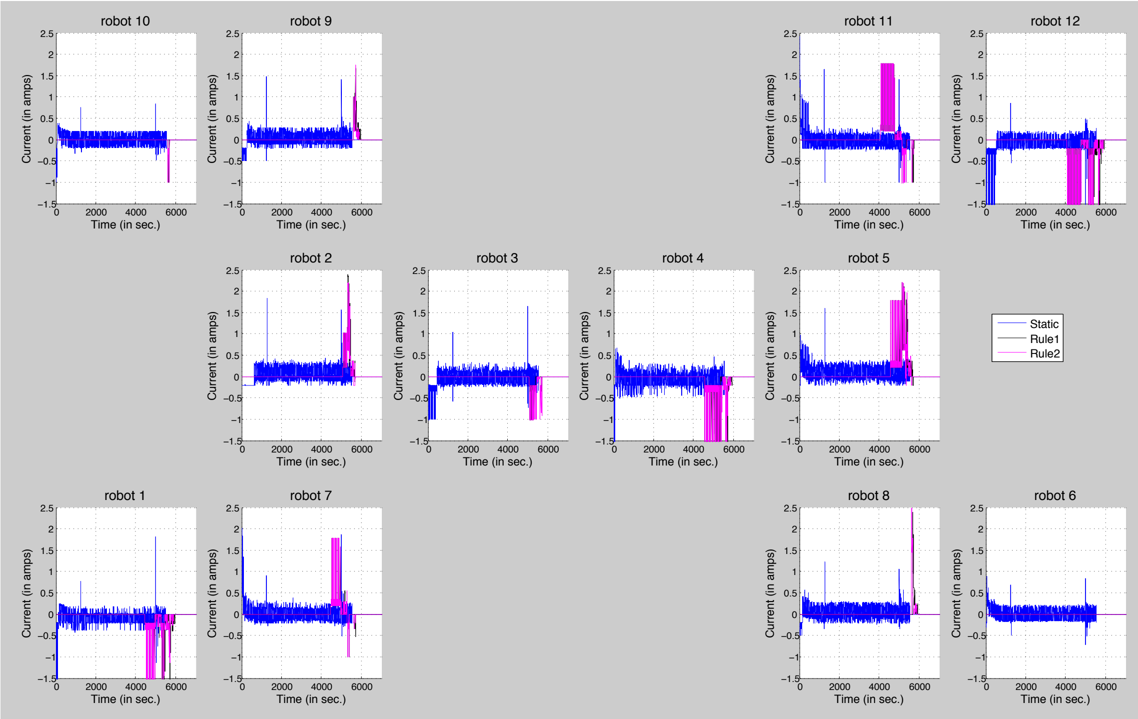

Figure 15: Energy sharing among the robotic modules of organism 2 measured at the power management energy sharing module with configuration C_2 and topology 1. The positive current values show the current flow into the system and vice versa. The horizontal axis shows the time scale in seconds and the vertical axis stands for current in amps. Each graph shows the measurements of *static* energy sharing in blue, *rule* 1 in black and *rule* 2 in magenta.

and 24 mA at the nominal system voltage. But the current losses with *rule* 1 and *rule* 2 energy sharing increased slightly compared to the earlier scenarios.

In the next two simulation runs the locomotion in organism 2 with uneven energy distribution was simulated with uneven mechanical load distributions among the robotic modules. Fig. 18 shows the energy sharing among the robotic modules of organism 2 measured at the power management energy sharing module with the configuration C_4 and topology-2. The organism in this scenario was able to cover 125 motion steps with *static* energy sharing, 115 motion steps with *rule* 1, and 124 motion steps with *rule* 2 energy sharing scheme. In regards to the covered motion steps, the *static* energy sharing produces nearly the same as with *rule* 2 energy sharing scheme. In the later two energy sharing scenarios – *rule* 1 and *rule* 2, sub-power buses in the organism were formed noticeably between r1 and r7, r9 and r10, r6 and r8, r5 and r4 and r11 and r12. Concerning energy losses fig. 20e shows the current losses in the three energy distribution scenarios. During *static* energy sharing scheme the current losses varied roughly between 14 mA and 20 mA at the nominal system voltage. While in the other two energy sharing schemes, the comparable current losses appeared only before the end of the simulation runs. In this case, we may conclude that the organism performance was almost equal in the two energy sharing schemes, i.e., uncontrolled and controlled energy sharing.

At the end, fig. 19 shows the energy sharing among the robotic modules of organism 2 measured at the power management energy sharing module with the configuration C_4 and topology-3. The organism in this scenario had covered 154 motion steps with *static* energy sharing, 150 motion steps with *rule* 1, and 149 motion steps with *rule* 2 energy sharing scheme. Again concerning the covered motion step, *static* energy sharing was empirically better then the later two cases. Fig. 20f shows the current losses during energy sharing in case C_4 and topology 3. In *static* energy sharing scheme the current losses varied roughly between 14 mA and 19 mA at the nominal system voltage. Whereas, in the later two cases the current losses increased in the later half of the simulation run.

A detailed analysis of the plots – of current losses, shown in fig. 20 reveal the system behavior in the two energy

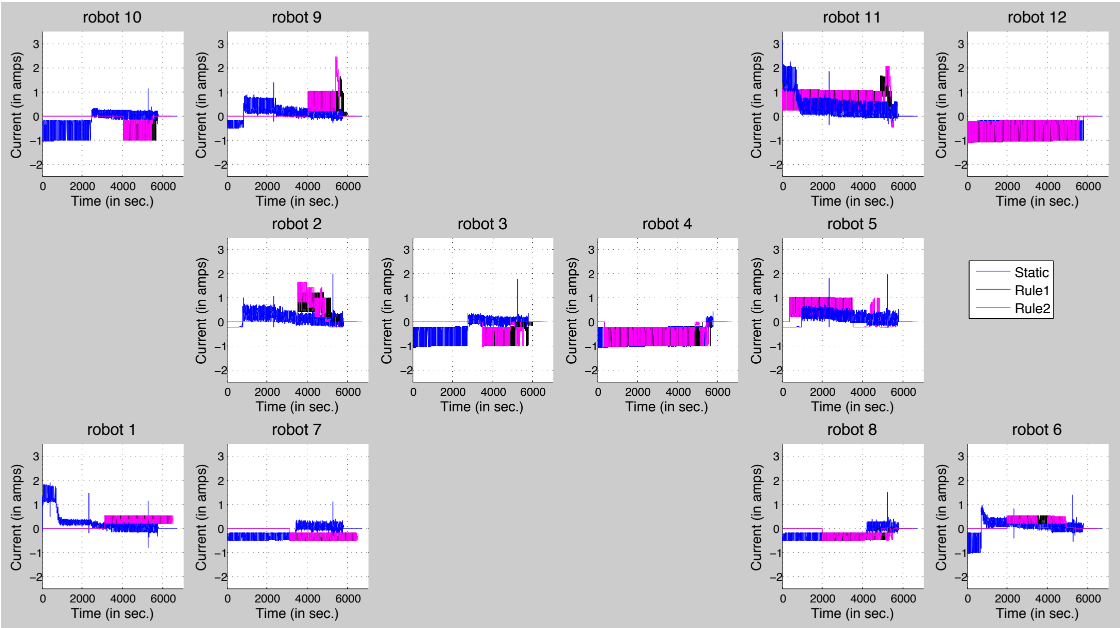

Figure 16: Energy sharing among the robotic modules of organism 2 measured at the power management energy sharing module with configuration C_3 and topology 2. The positive current values show the current flow into the system and vice versa. The horizontal axis shows the time scale in seconds and the vertical axis stands for current in amps. Each graph shows the measurements of *static* energy sharing in blue, *rule* 1 in black and *rule* 2 in magenta.

distribution topologies. Consider the initial energy distribution in case of topology-2, if the organism-2 is divided from the center, i.e., between r3 and r4, into two halves/segments, then the placement of energetically healthier robotic modules, i.e., r1, r11, r2, r9, r6 and r5 partially equalize the energy distribution or create a balance in the two halves of organism-2. This partially uniform energy distribution reduces the current losses in our controlled energy sharing scenarios as can be seen in fig. 20c and 20e. Now consider the initial energy distribution in case of topology-3, where the energy distribution in the organism creates an imbalance between the two segments/halves. More specifically, the energy was concentrated in the right half of the organism. This imbalance in energy distribution had slightly increased the energy losses during controlled energy sharing in organism 2 as can be seen in fig. 20d and 20f.

9. Summary and Conclusion

In this paper, firstly, we had pointed out some of the essential system features that play a critical role in controlling and managing the energy autonomy of autonomous robotic modules collectively in an organism. After that we had presented the design of a dynamic power management system with energy sharing ability especially developed for REPLICATOR robotic modules. Then the paper presents the experiments conducted with the real hardware to evaluate the individual and collective system behavior in different operating conditions. At the end, the paper presents a new simulation framework – *REPLICATOR power flow simulator*, with simulated results. The simulation framework was especially designed to simulate the dynamic energy sharing in a multi-robotic organism. For a controlled and uncontrolled power flow in a multi-robotic organism, the simulation framework defines the energy sharing schemes / mechanism along the motion models for two types of organisms.

In the absence of sufficient number of REPLICATOR robotic modules, the first phase of experiments with the real REPLICATOR hardware had provided us the solid ground to explore the collective system behavior in a simulation framework with varying set of parameters. From the simulation runs we have explored the collective behavior of robotic modules docked in the organism in different scenarios with varying configurations. From the empirical results obtained with two different type of organisms it is evident that the *static* energy sharing – single organism's power

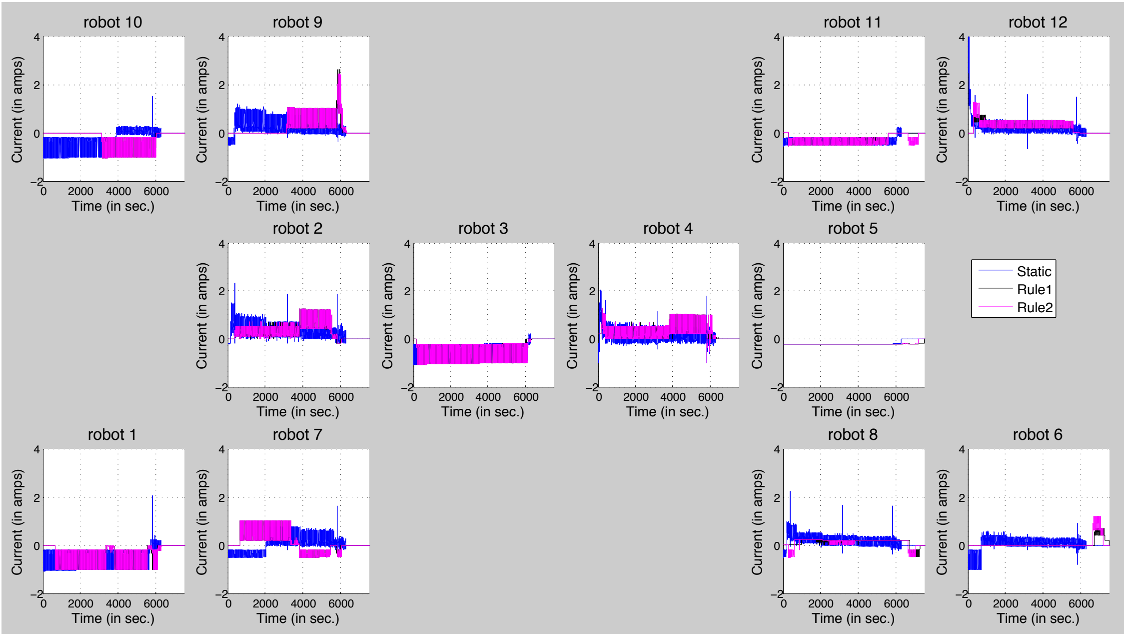

Figure 17: Energy sharing among the robotic modules of organism 2 measured at the power management energy sharing module with configuration C_3 and topology 3. The horizontal axis shows the time scale in seconds and the vertical axis stands for current in amps. Each graph shows the measurements of *static* energy sharing in blue, *rule* 1 in black and *rule* 2 in magenta.

bus with uncontrolled power flow, enabled the organism to cover more motion steps then our proposed controlled dynamic power sharing schemes. But it involves several complications. For instance, with *static* energy sharing where the energetically healthy robotic modules in the organism quickly loose their energy reserve, in case of reassembly – segregation of robotic modules from the organism, due to any reason, e.g., an abrupt system fault/failure in a robotic module, the previously energetic robotic modules may have lost their energetic autonomy. Where as, the proposed power sharing schemes – *rule* 1 and *rule* 2, enable the robotic modules to conserve their energy and allow them to share only when in the collective benefit. Another significantly important finding of the simulation is the importance of initial energy distribution in the organism. We have observed and discussed the effects of balanced and unbalanced initial energy distribution in the organism. From the simulation results we have concluded that it's significance should be considered during organism formation in the arena, i.e., how should the robotic modules dock themselves in the organism with respect to their energetic status. At the end, last but not least, the ultimate parameter to judge the efficiency of a particular energy sharing scheme is not the covered maximum distance or the operational time by the organism rather it may be the efficient energy utilization that allows the robotic modules to cope with internal and external uncertainties by keeping their energetic autonomy.

In our future work, to support our findings until now we have planned to explore the collective system behavior in a more complex organism structure.

10. ACKNOWLEDGMENTS

We would like to express our acknowledgment to Timo Koch who was of extremely big help in many hardware issues. This work is part of a European Union funded project named "REPLICATOR". The "REPLICATOR" project is funded within the work program Cognitive Systems, Interaction, Robotics under the grant agreement no. 216240.

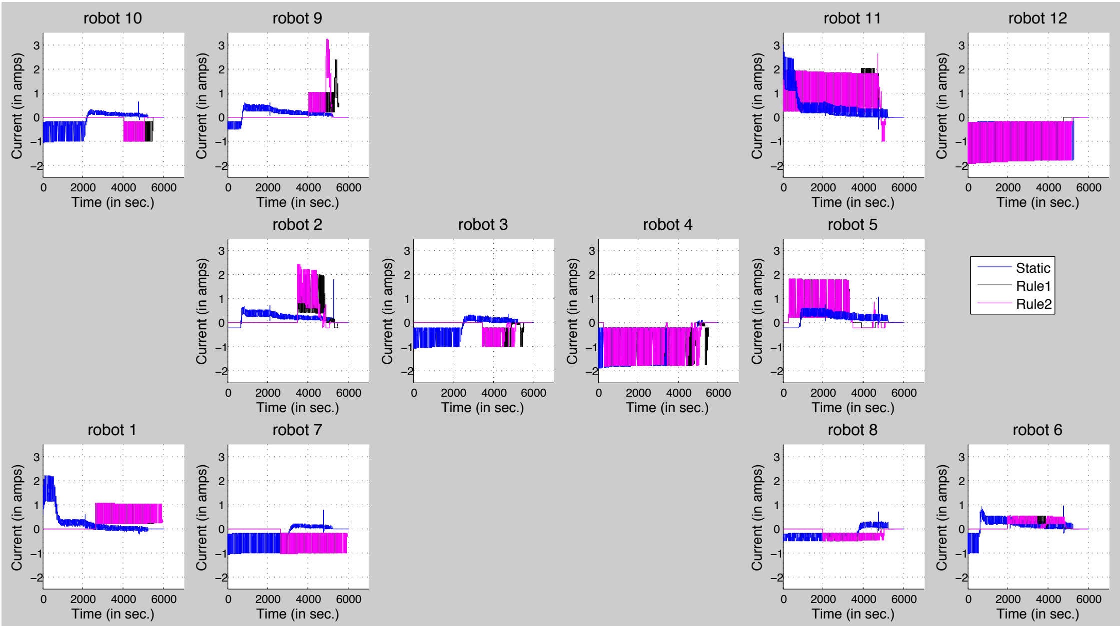

Figure 18: Energy sharing among the robotic modules of organism 2 measured at the power management energy sharing module with configuration C_4 and topology 2. The positive current values show the current flow into the system and vice versa. The horizontal axis shows the time scale in seconds and the vertical axis stands for current in amps. Each graph shows the measurements of *static* energy sharing in blue, *rule* 1 in black and *rule* 2 in magenta.

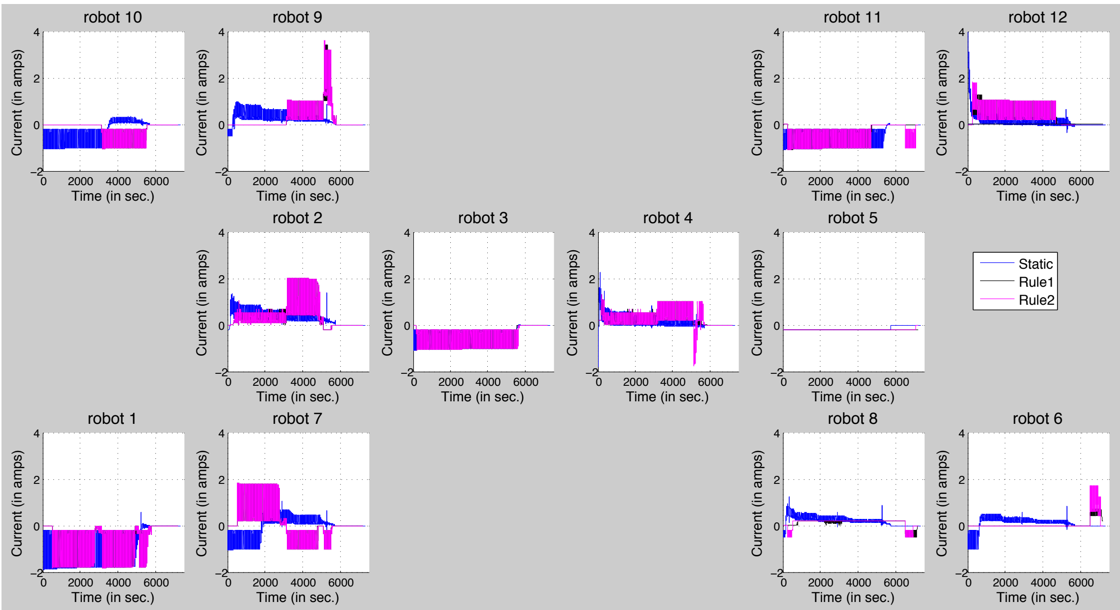

Figure 19: Energy sharing among the robotic modules of organism 2 measured at the power management energy sharing module with configuration C_4 and topology 3. The positive current values show the current flow into the system and vice versa. The horizontal axis shows the time scale in seconds and the vertical axis stands for current in amps. Each graph shows the measurements of *static* energy sharing in blue, *rule* 1 in black and *rule* 2 in magenta.

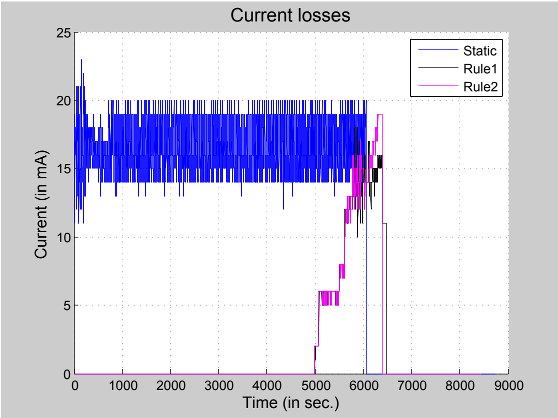

(a) In case C_1 and topology 1

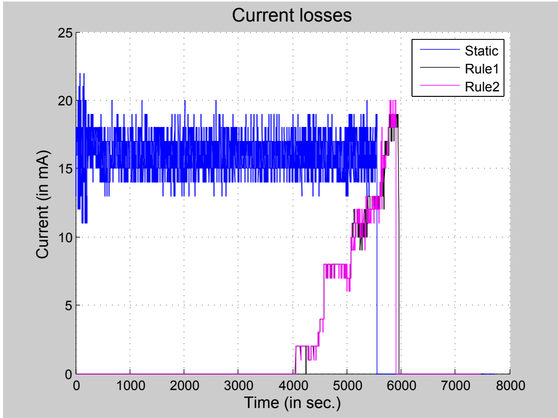

(b) In case C_2 and topology 1

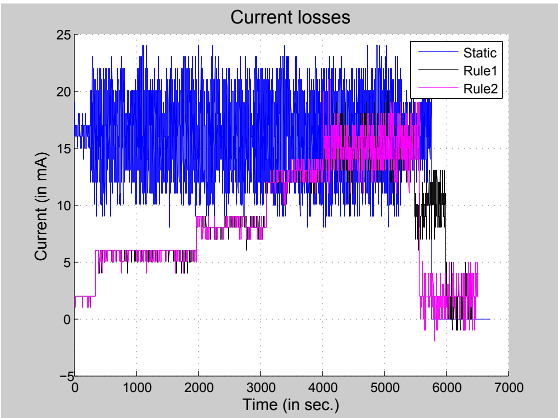

(c) In case C_3 and topology 2

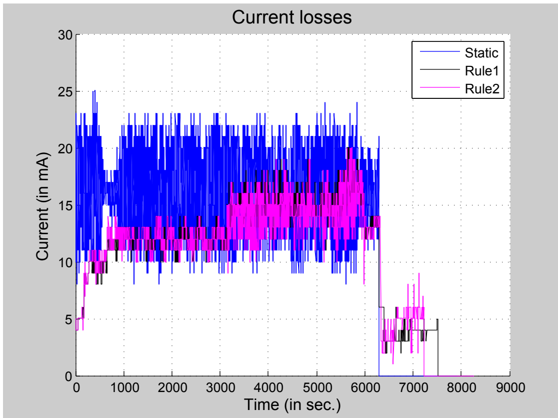

(d) In case C_3 and topology 3

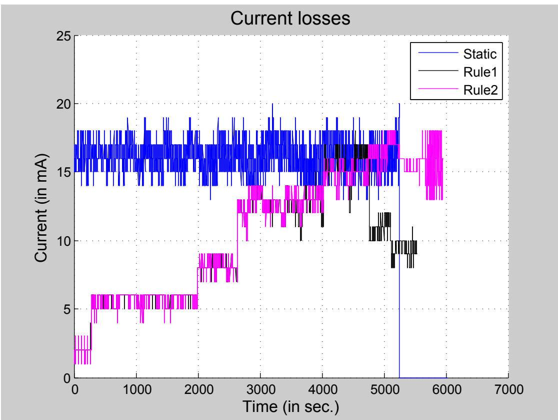

(e) In case C_4 and topology 2

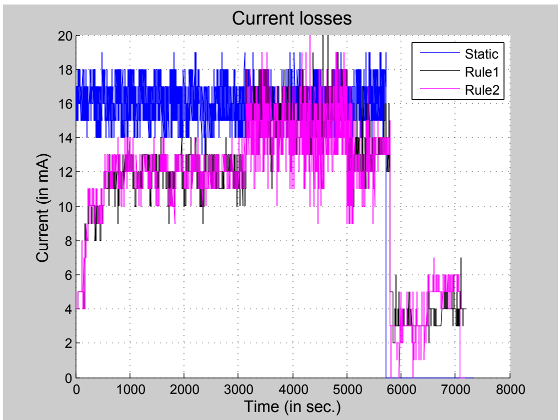

(f) In case C_4 and topology 3

Figure 20: Current losses during energy sharing in different scenarios. The horizontal axis in the plots show the time scale in seconds and the vertical axis stands for current in mA. Each graph shows the measurements of *static* energy sharing in blue, *rule* 1 in black and *rule* 2 in magenta.

References

[1] G. Estrin, B. Bussell, R. Turn, J. Bibb, Parallel processing in a restructurable computer system, IEEE Transactions on Electronic Computers EC-12 , Issue: 6 (1963) 747 – 755.
[2] G. Estrin, Organization of computer systems – the fixed plus variable structure computer, in: Western Joint Computer Conference, IRE-AIEE-ACM ’60 (Western), ACM, New York, NY, USA, 1960, pp. 33–40.
[3] M. Blanke, M. Kinnaert, J. Lunze, M. Staroswiecki, Introduction to diagnosis and fault-tolerant control, Springer Berlin Heidelberg, 2006, pp. 1–32.
[4] T. Fukuda, S. Nakagawa, Approach to the dynamically reconfigurable robotic system, Journal of Intelligent and Robotic Systems 1 (1988) 55–72.
[5] D. McFarland, Autonomy and self-sufficiency in robots, in: L. Steels, R. Brooks (Eds.), The Artificial Life Route To Artificial Intelligence: Building Embodied Situated Agents, Lawrence Erlbaum, USA, 1994, pp. 187–213.
[6] T. D. Ngo, Towards sociable robots – beyond energy autonomy, Ph.D. thesis, Department of Electronic Systems, Aalborg University, Denmark (2008).
[7] S. Yuta, Y. Hada, Long term activity of the autonomous robot - proposal of a bench-mark problem for the autonomy, in: Proceedings of the 1998 IEEE/RSJ Intl. Conference on Intelligent Robots and Systems, 1998, pp. 1871–1878.
[8] A. Barili, M. Ceresa, C. Parisi, Energy-saving motion control for an autonomous mobile robot, in: International Symposium on Industrial Electronics, 1995, pp. 674–676.
[9] F. M. Silva, J. A. T. Machado, Energy analysis during biped walking, in: IEEE International Conference on Robotics and Automation, Proceedings, Vol. 1, 1999, pp. 59–64.
[10] F. Yamasaki, K. Hosoda, M. Asada, An energy consumption-based control for humanoid walking, in: International Conference on Intelligent Robots and Systems (IROS), 2002, pp. 2473–2477.
[11] I. Duleba, J. Z. Sasiadek, Nonholonomic motion planning based on newton nonholonomic motion planning based on newton algorithm with energy optimization, in: IEEE Transactions on Control Systems Technology, Vol. 11(3), 2003, pp. 335–363.
[12] Y. Mei, Y. H. Lu, C. G. Lee, Y. C. Hu, Energy-efficient motion planning for mobile robots, in: International Conference on Robotics and Automation (ICRA), 2004, pp. 4344–4349.
[13] Y. Mei, Y. H. Lu, C. G. Lee, Y. C. Hu, Energy-efficient mobile robot exploration, in: IEEE International Conference on Robotics and Automation (ICAR), 2006, pp. 505–511.
[14] R. Humza, O. Scholz, A case study on self-sufficiency of individual robotic modules in an arena with limited energy resources, in: ADAPTIVE 2011, The Third International Conference on Adaptive and Self-Adaptive Systems and Applications, IARIA, 2011, pp. 39–35.
[15] B. Salemi, M. Moll, W.-M. Shen, Superbot: A deployable, multi-functional, and modular self-reconfigurable robotic system, in: IEEE/RSJ Intl. Conf. Intelligent Robots Systems, 2006, pp. 3636–3641.
[16] S. Murata, E. Yoshida, A. Kamimura, H. Kurokawa, M-tran: self-reconfigurable modular robotic system, in: IEEE/ASME Transactions on Mechatronics, Vol. 7, 2002, pp. 431–441.
[17] H. H. Lund, R. Beck, L. Dalgaard, Atron hardware modules for self-reconfigurable robotics, in: Sugisaka, Takaga (Eds.), Proceedings of the 10th International Symposium on Artificial Life and Robotics (AROB’10), Oita, Japan, 2005.
[18] E. H. Østergaard, Distributed control of the atron self-reconfigurable robot, Ph.D. thesis, Maersk McKinney Moller Institute for Production Technology, University of Southern Denmark (Nov. 2004).
[19] M. W. Jørgensen, E. H. Østergaard, H. H. Lund, Modular atron: Modules for a self-reconfigurable robot, in: Proceedings of 2004 IEEE/RSJ International Conference on Intelligent Robots and Systems (IROS), Sendai, Japan, 2004, pp. 2068–2073.
[20] S. Kernbach, F. Schlachter, R. Humza, J. Liedke, S. Popesku, S. Russo, T. Ranzani, L. Manfredi, C. Stefanini, R. Matthias, C. Schwarzer, B. Girault, P. Alschbach, E. Meister, O. Scholz, Heterogeneity for increasing performance and reliability of self-reconfigurable multi-robot organisms, in: CoRR, Vol. abs/1109.2288, 2011.
[21] L. Winkler, H. Wörn, Symbricator3d – a distributed simulation environment for modular robots, in: M. Xie, Y. Xiong, C. Xiong, H. Liu, Z. Hu (Eds.), Intelligent Robotics and Applications, Vol. 5928 of Lecture Notes in Computer Science, Springer Berlin / Heidelberg, 2009, pp. 1266–1277.